THE UNIVERSITY OF CHICAGO

ONE-ELECTRON THEORIES FROM THE GENERALIZED PAULI EXCLUSION PRINCIPLE

A DISSERTATION SUBMITTED TO
THE FACULTY OF THE DIVISION OF THE PHYSICAL SCIENCES
IN CANDIDACY FOR THE DEGREE OF
DOCTOR OF PHILOSOPHY

DEPARTMENT OF CHEMISTRY

BY
ROMIT CHAKRABORTY

CHICAGO, ILLINOIS
AUGUST 2017

I know the pieces fit

TABLE OF CONTENTS

LIST OF FIGURES

LIST OF TABLES

ABSTRACT

The Pauli Exclusion Principle ensures that orbital occupations arise from a physically realistic quantum system. There are additional conditions, motivated by quantum information theory, that are necessary for electron occupations to arise out of pure quantum states that are said to generalize the Pauli principle. Our work with Generalized Pauli conditions has lead us to develop electronic structure theories that are able to, *i*) recover many-body correlation energies, *ii*) derive sufficient conditions for openness in a quantum system, *iii*) formulate a geometric perspective on energy transfer, and, *iv*) highlight the structural complexity of excited state spectra, from one-electron theories.

ACKNOWLEDGMENTS

When I arrived here, I quickly realized that scientific training in US is more intuitive compared to the analytical training I was used to. It was obvious that while abstract thought is essential for theory, the feel for problems must have a perceptual precedent, the principal reason research conducted here lies at the frontiers of science and is able to take on big questions of our day and age. Needless to say, it has been an immense privilege to be able to live and work in the hallowed precincts of the University of Chicago, the spiritual home of theoretical chemistry. I might have taken the 'living a dream' part too literally with frequent overnight sojourns at my office at The James Franck Institute. Something about the quietness of campus in the middle of the night, the muffled sirens of frequent police cars in snow-filled winter nights, will make me look back fondly at years of solitary work at the university.

I am grateful to David for being a constant guiding presence, and for rekindling my spirit of intellectual curiosity. I worked hard, and David encouraged me every step of the way, and it is his childish curiosity for numerical problems that made me think I would one day rediscover mine. As I step onto a new academic life, my wish is to be able to enjoy, more simply, the joys of working on a problem.

We were brought up in a scholarly tradition where discipline in academic pursuits was paramount. My family values, above all else, the significance of intellectual traditions and its necessary sacrifice. I am thankful to my father, for being the bedrock of our family, my mother for her love and her taste in the arts, my brother for introducing me to music, and to cricket, and to my grandmother for raising me. It is the dedication and authenticity of our parents' generation that has enabled the current crop strong-willed and confident Indians to take on the world.

My experiences at the University of Chicago would have been incomplete without friends I have the good fortune of making. Paul (Jonathan Sanstead) was a calming presence, along with the pints of lager, or Guinness, or margaritas that we were usually accompanied by. I

discovered squash here. A close group of friends - Sunny (Chatterjee), Glen (Hocky), Nishq (Mody), Ronen (Mukamel), Marc (Gillard), Jack (Shotton), Ish (Dawra), Fahad (Sajid) have reveled in our aerobic capacities (or the lack thereof) at Henry Crown for longer than we should have, taking ourselves more seriously that we ought to have. Gamma Alpha opened its doors for me, and while I survived mostly on soylent, UFG food never hurts. Min, Becky, Taeju, Gerry, Saul, and Tanima were always around for an uplifting chat, not to mention Abhishek, and the cosmic conspiracy out to reunite us.

Dave (Schuster) and Srivatsan, who were working on a quantum RAM right under our feet at the JFI were enormously receptive on any input we had on measuring natural orbital occupations over coffee-machine chats. It is hard not to be infected by Professor Engel's energy and Professor Tian's charm while you are at the JFI. Tim (Berkelbach) made prescient observations on this thesis concerning the need for consideration of size-extensivity of GPC-inspired electronic structure theories. Finally, I would like to thank Christian (Schilling), Carlos (Benevides-Riveros), Felix (Tennie), Nicole (Helbig), and Nektarios (Lathiotakis) for fruitful conversations during our trip to Oxford.

CHAPTER 1

THE GENERALIZED PAULI EXCLUSION PRINCIPLE

This chapter contains excerpts from the following published articles:

- Reproduced from [R. Chakraborty and D. A. Mazziotti, *Phys. Rev. A*, **89**, 042505 (2014)]. Copyright 2014, American Physical Society.
- Reproduced from [R. Chakraborty and D. A. Mazziotti, *Phys. Rev. A*, **91**, 010101 (2015)]. Copyright 2015, American Physical Society.
- Reproduced from [R. Chakraborty and D. A. Mazziotti, *Int. J. Quantum Chem.*, **116**, 784 (2016)]. Copyright 2016, John Wiley and Sons.
- Reproduced from [R. Chakraborty and D. A. Mazziotti, *J. Chem. Phys.*, **146**, 184101 (2017)]. Copyright 2017, American Institute of Physics.

1.1 Introduction

The *Pauli exclusion principle* states that two identical fermions cannot occupy the same quantum state [1]. Postulated by Pauli in 1925 to explain atomic transitions [2], this principle plays a key role in predicting electronic configurations of atoms and molecules. Stated otherwise, the Pauli principle says that the fermion occupation numbers λ_i of a quantum system must lie between 0 and 1

$$0 \leq \lambda_i \leq 1. \tag{1.1}$$

Subsequent work by Dirac [3] and Heisenberg [4] showed that this principle arises from the antisymmetry of the fermion wave function.

As discussed by von Neumann [5], a general N-fermion quantum state is expressible by

an N-fermion ensemble density matrix

$$^{N}D(1,2,..,N;\bar{1},\bar{2},..,\bar{N}) = \sum_{i} w_i \Psi_i(1,2,..,N)\Psi_i^*(\bar{1},\bar{2},..,\bar{N}) \tag{1.2}$$

where w_i are non-negative weights that sum to unity, $\Psi_i(1,2,..,N)$ are N-fermion wave functions, and each number denotes the spatial and spin coordinates of a fermion. Integration of the N-fermion *ensemble density matrix* over the coordinates of all fermions save one yields the one-fermion reduced density matrix (1-RDM)

$$^{1}D(1;\bar{1}) = \int {}^{N}D(1,2,..,N;\bar{1},2,..,N)d2d3..dN. \tag{1.3}$$

Like the N-fermion density matrix, the 1-RDM must be (i) Hermitian, (ii) normalized, and (iii) positive semidefinite. However, the 1-RDM must also obey additional constraints to ensure that it is derivable from the integration of an N-fermion ensemble density matrix ^{N}D. These additional constraints are known as *ensemble N-representability conditions* [6]. The eigenfunctions of the 1-RDM are known as *natural orbitals* while the eigenvalues of the 1-RDM are known as the *natural occupation numbers*. Coleman showed that the Pauli exclusion principle applied to the natural occupation numbers imposes necessary and sufficient ensemble N-representability conditions on the 1-RDM, that the eigenvalues of the 1-RDM must lie between 0 and 1 [6]. While the Pauli conditions of the 1-RDM are complete ensemble N-representability conditions, additional conditions on the 1-RDM are required to ensure that it arises from the integration of an N-fermion *pure density matrix*

$$^{N}D(1,2,..,N;\bar{1},\bar{2},..,\bar{N}) = \Psi(1,2,..,N)\Psi^*(\bar{1},\bar{2},..,\bar{N}) \tag{1.4}$$

where the ^{N}D can be spectrally resolved in terms of the single N-fermion wave function $\Psi(\bar{1},\bar{2},..,\bar{N})$. These additional 1-RDM constraints are known as *pure N-representability conditions* or *generalized Pauli conditions* [6–11]. The pure N-representability conditions

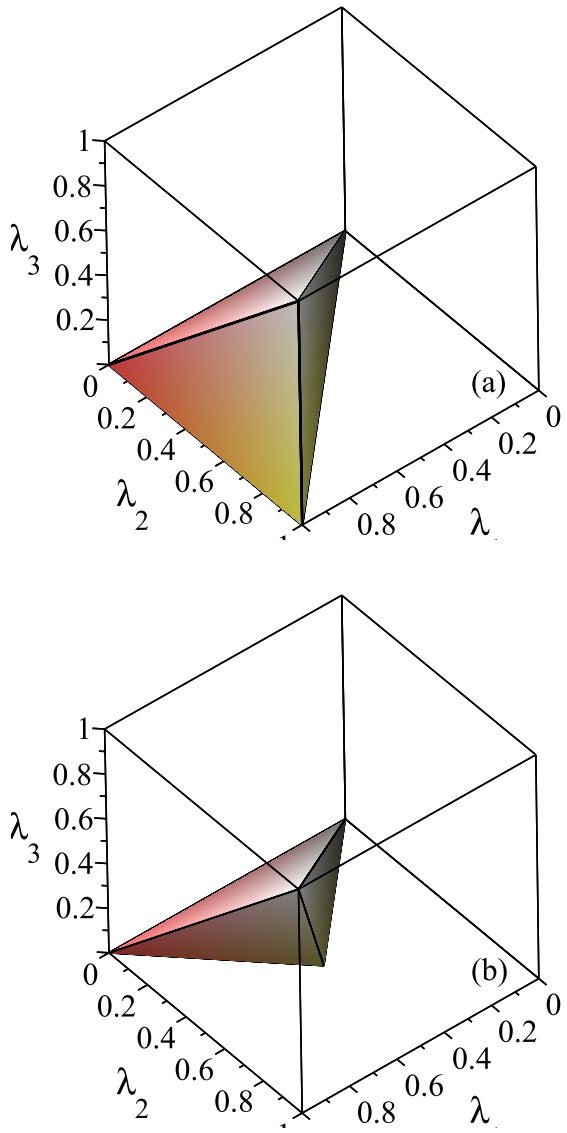

Figure 1.1: The sets of (a) ensemble and (b) pure N-representable 1-RDMs are shown for a general three-electron ($N = 3$) and six-orbital ($r = 6$) quantum system. The plane defined by the Borland-Dennis equalities in Eq. (1.6) causes the pure N-representable set of 1-RDMs in (b) to be significantly smaller than the ensemble N-representable set of 1-RDMs in (a). The sets are shown in terms of the first three natural occupation numbers, λ_1, λ_2, and λ_3, ordered from highest to lowest, relative to a fixed set of natural orbitals. These three occupation numbers provide a complete three-dimensional description of the pure 1-RDM spectra because the other occupation numbers are determined from the Borland-Dennis equalities in Eq. (1.5); they provide a partial description of the full five-dimensional ensemble 1-RDM spectra.

of the 1-RDM depend only on its natural occupation numbers [6], and hence, we will use the terms N-representability of the 1-RDM and N-representability of the 1-RDM spectrum,

interchangeably. Smith showed that pairwise degeneracy of occupation numbers are sufficient to ensure pure N-representability of the 1-RDM [7]. Furthermore, he showed that such degeneracy occurs naturally in even-N quantum systems with time-reversal symmetry. In 1972 Borland and Dennis reported pure N-representability conditions for active space of three fermions in six orbitals denoted by $\wedge^3[\mathcal{H}_6]$, on the basis of numerical calculations [8]. For an ordered set of occupation numbers $\lambda_i \geq \lambda_{i+1}$, their conditions are given by

$$\lambda_1 + \lambda_6 = \lambda_2 + \lambda_5 = \lambda_3 + \lambda_4 = 1 \tag{1.5}$$

$$\lambda_5 + \lambda_6 - \lambda_4 \geq 0. \tag{1.6}$$

Until recently, a systematic enumeration of generalized Pauli constraints has been elusive. Based on work in quantum marginal theory, Klyachko was able to list the necessary and sufficient constraints for N fermions in r orbitals [9]. These constraints are expressible in the form of linear inequalities in the occupation numbers $\{\lambda_i\}$

$$\kappa_0 + \kappa_1 n_1 + \cdots + \kappa_r n_r \geq 0, \tag{1.7}$$

which can be visualized as a convex polytope in $\mathbb{R}^r$. The polytope for $N = 3$ and $r = 6$, whose boundary is defined by the Borland-Dennis inequalities in Eqs. (1.5) and (1.6), is shown in Fig. 1.1.

We outline the pure N-representability problem in section 1.2, and define metrics to asses constraint saturation in by 1-RDM spectra in section 1.3. 1-RDM pure N-representability conditions for finite Hilbert spaces given by Klyachko [9, 46] gives rise to selection rules for N-electron configurations (determinants) that may contribute to wavefunctions that lie on the boundary of the set of pure N-representable 1-RDMs. Physical systems that are found to quasi-saturate (*quasipin*) these 1-RDM pure N-representability conditions can be reconstructed from the set of extremal 1-RDMs, giving correlated many-fermion energies from single-party information. In section 1.6 we derive theorems that are sufficient to certify

openness of a many-electron quantum system from knowledge of its occupation spectrum, finally finishing with structural simplifications for pure-state representability constraints for a system of N qubits in section 1.7.

1.2 The Pure N-Representability Problem

Pure N-representability conditions are able to distinguish between pure and ensemble (mixed) quantum systems from their reduced descriptions. The density matrix ${}^{N}D$ for a pure N-fermion quantum state $|\Psi_N(1\cdots N)\rangle$ is given by the outer product $\Psi_N(1\cdots N)\Psi_N^*(\bar{1}\cdots\bar{N})$ of the wavefunction and has information about spatial and spin co-ordinates of N particles. Any measurement on the quantum state realizes copies $|\Psi_i\rangle$ of the wavefunction resulting in an ensemble (mixture) of quantum states whose density matrix ${}^{N}D$ is now given by

$$ {}^{N}D(1\cdots N;\bar{1}\cdots\bar{N}) = \sum_i w_i \Psi_i(1\cdots N)\Psi_i^*(\bar{1}\cdots\bar{N}), \tag{1.8}$$

where w_i's are non-negative weights that sum to unity. Integrating ${}^{N}D$ over all co-ordinates but one gives the one-electron reduced density matrix (the 1-RDM)

$$ {}^{1}D(1;\bar{1}) = \int {}^{N}D(1,2,\cdots,N;\bar{1},2,\cdots,N)d2d3\cdots dN, \tag{1.9}$$

which, like its N-particle counterpart, must be Hermitean, normalized and positive semi-definite [12, 13]. In the finite dimensional one-particle Hilbert space $\wedge^N\mathcal{H}_r^{(1)}$, the 1-RDM is diagonalizable with a suitable unitary transformation

$$ U^{-1}({}^{1}D)U \equiv \sum_{j=1}^{r} n_j |j\rangle\langle j|, \tag{1.10}$$

giving as its eigenfunctions of natural orbitals and as its eigenvalues, the natural orbital occupations $\{n_j, j = 1,\cdots,r\}$ that give the probability of finding an electron in the jth

spin orbital for all possible configurations of the other $(N-1)$ electrons. Coleman showed in 1963 that the N-representability problem is invariant under unitary transformations and that representability criteria for reduced descriptions of a quantum system may be written in terms of eigenvalues of its reduced density matrices [6, 14]. He showed furthermore that the Pauli Exclusion principle, which bounds fermion occupations between zero and one, is necessary and sufficient to ensure that electron occupations arise from at least one physically realizable N-electron ensemble density matrix [1, 2, 4, 6, 15]. This *ensemble N-representability* criterion defines the set $\mathcal{E}^1_{N,r}$ of physically realistic ensemble 1-RDMs that are derivable from the N-particle density matrix. Additional conditions apply on election occupations that arise out of pure quantum states that are said to generalize the Pauli principle [7–9, 16]. Borland and Dennis were able to enumerate these constraints for three electrons in six spin orbitals (the state space $\wedge^3\mathcal{H}_6$) in 1972 while working as computer scientists at IBM [8]. In their pathbreaking work from 2006-2008, Klyachko and Ahltunbalak formulated an algorithm to solve for these constraints using Schubert calculus to enumerate single-particle marginals of symmetric permutation groups in Lie algebra [9, 46].

These *pure N-representability* conditions are affine inequalities

$$\langle {}^1\hat{O}_c\rangle = \kappa_0 + \sum_{j=1}^{r} \kappa_j n_j \geq 0 \tag{1.11}$$

on the monotonically decreasing spectrum of natural orbital occupations $\{n_j, n_j \geq n_{j+1}\}$; κ's are integer constants and ${}^1\hat{O}_c$ is the single particle operator whose expectation value gives a measurable definition for constraint saturation for single-particle spectra [10–13, 17–22]. For the finite dimensional single-particle Hilbert space $\wedge^N\mathcal{H}^{(1)}_r$ there are n_c such constraints that define the set of generalized Pauli conditions (GPCs) $B^1_{N,r}$ for a given single-particle basis. The set $\mathcal{P}^1_{N,r}$ of pure N-representable 1-RDMs comprises of $1-$RDMs that obey

inequalities (1.11),

$$\mathcal{P}^1_{N,r} = \left\{ {}^1D | \, \mathrm{Tr}({}^1\hat{O}_c \, {}^1D) \geq 0 \ \forall \ {}^1\hat{O}_c \in B^1_{N,r} \right\}, \tag{1.12}$$

and contains all 1-RDMs that have at least one wavefunction pre-image [12, 13, 17, 21, 23]. Geometrically, $\mathcal{P}^1_{N,r}$ assumes a convex polytope in the space $\mathbb{R}^r$ of natural orbital occupations formed from the intersection of n_c hyperplanes, each representing a GPC facet [12, 13, 22] in $B^1_{N,r}$.

1.3 Spectral Pinning

In section 1.3.1 we discuss a necessary 2-RDM condition for pinning of the 1-RDM to the boundary of pure N-representable 1-RDMs. In section 1.3.2 we compute the minimum Euclidean distances to the boundaries of the sets of N-representable 1-RDMs that are pure and ensemble, respectively. These Euclidean distances are useful for both measuring and classifying electron correlation and entanglement. Finally, in section 1.3.3 we discuss the pure N-representable 1-RDM set for even-N quantum systems with time-reversal symmetry.

1.3.1 Necessary 2-RDM Condition

Spectral pinning of the 2-RDM is necessary for extremality of ground-state occupation spectra. This necessary criterion for 1-RDM pinning is investigated in Ref. [12] with supporting numerics on ground and excited states of atoms and molecules. The ground-state energy of an N-electron system can be expressed as a functional of the 2-RDM

$$E = \frac{N(N-1)}{2} \mathrm{Tr}({}^2K \, {}^2D) \tag{1.13}$$

where ${}^2D$ is the 2-RDM

$$ {}^2D(1,2;\bar{1},\bar{2}) = \int {}^N D(1,2,..,N;\bar{1},\bar{2},..,N) d3..dN \tag{1.14} $$

and ${}^2K$ is the two-electron reduced Hamiltonian

$$ {}^2K(1,2;\bar{1},\bar{2}) = \frac{1}{N-1}\sum_{i=1}^{2}(-\frac{1}{2}\hat{\nabla}_i^2 - \sum_k \frac{Z_k}{r_{ik}}) + \frac{1}{r_{12}}. \tag{1.15} $$

Minimization of the energy over the convex set E_N^2 of ensemble N-representable 2-RDMs yields the ground-state energy E_0 of the N-electron quantum system [6, 15]

$$ E_0 = \min_{{}^2D \in E_N^2} E({}^2D). \tag{1.16} $$

Because the energy is a linear functional of the 2-RDM, the optimal 2-RDM for a non-degenerate ground state lies on the boundary of the convex set E_N^2.

A 2-RDM that is *ensemble N-representable* must be derivable from the integration of at least one N-electron density matrix. The 2-RDM that is *pure N-representable* must also be derivable from the integration of at least one pure N-electron density matrix. From these definitions it follows that the set P_N^2 of pure N-representable 2-RDMs is contained in the set E_N^2 of ensemble N-representable 2-RDMs, that is $P_N^2 \subset E_N^2$. By the energy minimization discussed above, the 2-RDM of a non-degenerate ground state lies on the boundary of the ensemble set E_N^2. Because the 2-RDM of a non-degenerate ground state is pure N-representable and $P_N^2 \subset E_N^2$, it also lies on the boundary of the pure set P_N^2. In contrast, while an excited-state 2-RDM is pure N-representable, it generally lies *inside* the ensemble set E_N^2 of 2-RDMs.

Because a 1-RDM arises from the integration of a ground-state 2-RDM over the coordinates for electron two, the ground-state 1-RDM can lie in the boundary of its pure N-representable set P_N^1 only if it derives from a 2-RDM that lies on the boundary of its pure

N-representable set P^2_N. Hence, the 2-RDM contains a necessary condition for the pinning of the 1-RDM spectra to the generalized Pauli conditions. This result also provides important information about the potential difference in pinning of the ground-state and excited-state 1-RDM spectra. Because the ground-state 2-RDM lies on the boundary of the ensemble N-representable 2-RDM set E^2_N and hence, on the boundary of the pure N-representable 2-RDM set P^2_N, it is possible for the ground-state 1-RDM to lie on the boundary of the pure N-representable 1-RDM set P^1_N. In contrast, because an excited-state 2-RDM does not necessarily lie on the boundary of E^2_N or P^2_N, it may not be possible for the excited-state 1-RDM (of a given spin symmetry) to lie on the boundary of P^1_N.

1.3.2 Distance Metrics

Optimization programs for computing constraint saturation by 1-RDM spectra were developed (see Ref. [12]). The minimum Euclidean distance from a given 1-RDM's the r-dimensional spectrum of natural occupation numbers $\vec{n} = \{\lambda_i\}$ to three other points in the Euclidean space of spectra: (i) the nearest point $\vec{p}$ on the boundary of the set of *pure* N-representable 1-RDMs, (ii) nearest point $\vec{e}$ on the boundary of the set of *ensemble* N-representable 1-RDMs, and (iii) the nearest point $\vec{s}$ corresponding to a 1-RDM with a Slater determinant pre-image, were computed. These three distances are useful in assessing a quantum system's electron correlation as well as its purity. A quantum system is pure if and only if it is described by a single wave function rather than an ensemble of wave functions.

Firstly, we can compute the minimum distance of the spectrum $\vec{n}$ to the boundary of *pure* N-representability 1-RDMs or in other words the minimum distance of $\vec{n}$ to the polytope facets defined by the generalized Pauli conditions $M\vec{p} \geq b$, the Pauli conditions $0 \leq p_i \leq 1$, the trace condition $\sum_i p_i = N$, and a condition ordering the occupation numbers from highest to lowest in magnitude $p_{i+1} \leq p_i$ where $\vec{p}$ is any point in the d-dimensional Euclidean

space $\mathbb{R}^r$:

$$\min_j \min_{\vec{p}\in\mathbb{R}^r} ||\vec{n}-\vec{p}|| \tag{1.17}$$

$$\text{such that } \sum_i p_i = N \tag{1.18}$$

$$p_{i+1} \leq p_i \text{ for all } i \in [1, r-1] \tag{1.19}$$

$$\leq p_i \leq 1 \text{ for all } i \in [1, r] \tag{1.20}$$

$$M\vec{p} \geq b \tag{1.21}$$

$$\sum_i M_i^j p_i = b_j \tag{1.22}$$

The algorithm works by (i) minimizing the Euclidean distance to each facet j and (ii) minimizing over the results from (i). For $N = 3$ the constraints $M\vec{p} \geq b$ represent the Borland-Dennis constraints, and for $N = 4$ the constraints represent either the Klyachko or Smith constraints. We shall refer to the set of pure N-representable 1-RDMs as the *pure set* and the minimum Euclidean distance to the boundary of the pure set as the *pure distance*.

Secondly, we can compute the minimum Euclidean distance to the boundary of the set of ensemble N-representable 1-RDMs, defined by the Pauli principle and the trace condition, as follows:

$$\min_{j,b\in\{0,1\}} \min_{\vec{e}\in\mathbb{R}^r} ||\vec{n}-\vec{e}|| \tag{1.23}$$

$$\text{such that } \sum_i e_i = N \tag{1.24}$$

$$e_{i+1} \leq e_i \text{ for all } i \in [1, r-1] \tag{1.25}$$

$$0 \leq e_i \leq 1 \text{ for all } i \in [1, r] \tag{1.26}$$

$$e_j = b \tag{1.27}$$

where $\vec{e} = \{e_i\}$ is any point in the *ensemble set*. We shall refer to the minimum Euclidean distance to the boundary of the ensemble set as the *ensemble distance*.

Finally, the natural occupation numbers of a non-interacting 1-RDM, the 1-RDM that derives from a Slater determinant, are either fully occupied or empty. These eigenvalues defined the components of a Slater point $\vec{s}$ in Euclidean space

$$\vec{s} = (1, 1, \cdots, 0, 0). \tag{1.28}$$

The minimum Euclidean distance from a given 1-RDM's spectrum $\vec{n}$ to the nearest Slater point can be computed from the following minimization:

$$\min_{\vec{s} \in \mathbb{S}^r} ||\vec{n} - \vec{s}|| \tag{1.29}$$

where $\mathbb{S}^r$ denotes the set of all Slater points. The Euclidean distance $||\vec{n} - \vec{s}||$ of the spectrum from the Slater point gives a useful measure of electron entanglement and correlation that equals zero in the absence of correlation.

1.3.3 Time-Reversal Symmetry

As shown in Ref.[12], consideration of time-reversal symmetry is important in assessing spectral pinning. Smith proved two key results in the study of the pure N-representability conditions of the 1-RDM [7]. Firstly, for an even-N quantum state, if all of the eigenvalues of the state's 1-RDM are evenly degenerate, then the 1-RDM is pure N-representable. Secondly, if an even-N quantum state has time-reversal symmetry, then all of the eigenvalues of the state's 1-RDM are evenly degenerate. Hence, *if an even-N quantum state has time-reversal symmetry, the degeneracy of the eigenvalues of the 1-RDM is necessary and sufficient for the 1-RDM to be pure N-representable.*

Smith's set of pure N-representable 1-RDMs with time-reversal symmetry S_N^1 is a subset of the pure N-representable set of 1-RDMs P_N^1, that is $S_N^1 \subset P_N^1$. Importantly, any 1-RDM from a pure state with time-reversal symmetry is pinned to the boundary of the Smith set S_N^1. For example, for $N = 4$ and $r = 8$ the Smith set is characterized by the four equalities

between natural occupation numbers

$$\lambda_1 = \lambda_2 \tag{1.30}$$

$$\lambda_3 = \lambda_4 \tag{1.31}$$

$$\lambda_5 = \lambda_6 \tag{1.32}$$

$$\lambda_7 = \lambda_8. \tag{1.33}$$

Each equality can be viewed as two inequalities; for example, the first equality can be expressed as the following two inequalities

$$\lambda_1 \leq \lambda_2 \tag{1.34}$$

$$\lambda_2 \leq \lambda_1. \tag{1.35}$$

Because these inequalities are always saturated, any 1-RDM in the Smith set is pinned to the boundary of the Smith set. More generally, this result is true for any even N and r.

For $N = 4$ and $r = 8$ the generalized Pauli inequalities on the natural occupation numbers of the 1-RDM, determined computationally by Borland and Dennis [8] and derived by Klyachko [9], are

$$4 - \sum_{i=1}^{8} M_i^j \lambda_i \geq 0 \tag{1.36}$$

$$4 + \sum_{i=1}^{8} M_{9-i}^j \lambda_i \geq 0. \tag{1.37}$$

Seven sets of coefficients M_i^j are given in Table 1.1 for a total of 14 inequalities. When time-reversal symmetry is imposed on the 1-RDM by forcing its eigenvalues to be evenly degenerate, these generalized Pauli inequalities reduce to the traditional Pauli exclusion principle. Consequently, a 1-RDM with time-reversal symmetry is pinned to the Klyachko

Table 1.1: For $N = 4$ and $r = 8$ the generalized Pauli inequalities on the natural occupation numbers of the 1-RDM, shown in Eqs. 1.36 and 1.37, have seven sets of coefficients M_i^j displayed below where j labels the set and i labels the coefficient within a set.

	Coefficients in Eqs. (1.36) and (1.37)							
j	M_1^j	M_2^j	M_3^j	M_4^j	M_5^j	M_6^j	M_7^j	M_8^j
1	5	-3	1	1	1	1	-3	-3
2	5	1	-3	1	1	-3	1	-3
3	5	1	1	-3	1	-3	-3	1
4	5	1	1	-3	-3	1	1	-3
5	1	5	1	-3	1	-3	1	-3
6	1	1	5	-3	1	1	-3	-3
7	1	1	1	1	5	-3	-3	-3

inequalities if and only if it is pinned to the traditional Pauli conditions, meaning the boundary of the ensemble N-representable 1-RDM set. The 1-RDM with time-reversal symmetry has a spectrum that is typically not pinned to the convex Klyachko set P_N^1 because P_N^1 contains additional 1-RDMs than the convex Smith set S_N^1 that break time-reversal symmetry.

1.4 Selection Rules

The wavefunction of the N-fermion quantum system is a linear combination of all possible N-electron configurations (slater determinants) which can be written in the basis of natural orbitals as

$$|\Psi_N(1\cdots N)\rangle = \sum_{|s_k\rangle\in\mathcal{F}_{N,r}} c_k|s_k\rangle, \tag{1.38}$$

$$|s_k\rangle = \frac{\sigma_k}{\sqrt{N!}}\left(|j_1(1)\rangle \wedge |j_2(2)\rangle \wedge \cdots \wedge |j_r(r)\rangle\right), \tag{1.39}$$

where complex coefficients c_k are contributions due to each slater determinant $|s_k\rangle$ and natural orbitals $(\{|j_i\rangle, i = 1, \cdots, r\})$ are indexed such that their respective occupations $(\{n_i | n_i \geq n_{i+1}\, \forall\, i \in [1, (r-1)]\})$ are non-decreasingly ordered. Permutation operator σ generates the set of configurations $\mathcal{F}_{N,r}$ that contains $\binom{r}{N}$ determinants, encompassing all

Table 1.2: Selection rules for pinned spectra in the state space $\wedge^4\mathcal{H}_8$ for $M_z = 0$ shows slater determinants that contribute to 7 unique GPC facets. Constraints $\{1, 2, 3\}$ are pinned by 10 determinants while $\{4, 5, 6, 7\}$ are pinned by 9, compared to 36 possible determinants with $M_z = 0$.

p	Operator (${}^1\hat{\mathrm{O}}_\mathrm{p}$)	Pinned Determinants (∂P_p^1)
1	$\hat{a}_6^\dagger\hat{a}_6 + \hat{a}_7^\dagger\hat{a}_7 + \hat{a}_8^\dagger\hat{a}_8 - \hat{a}_5^\dagger\hat{a}_5$	$\{\|1234\rangle, \|1458\rangle, \|1256\rangle, \|1356\rangle, \|1257\rangle, \|1357\rangle, \|2456\rangle, \|3456\rangle, \|2457\rangle, \|3457\rangle\}$
2	$\hat{a}_2^\dagger\hat{a}_2 + \hat{a}_7^\dagger\hat{a}_7 + \hat{a}_8^\dagger\hat{a}_8 - \hat{a}_1^\dagger\hat{a}_1$	$\{\|1234\rangle, \|1236\rangle, \|1245\rangle, \|1256\rangle, \|1357\rangle, \|3456\rangle, \|1348\rangle, \|1368\rangle, \|1458\rangle, \|1568\rangle\}$
3	$\hat{a}_4^\dagger\hat{a}_4 + \hat{a}_7^\dagger\hat{a}_7 + \hat{a}_8^\dagger\hat{a}_8 - \hat{a}_3^\dagger\hat{a}_3$	$\{\|1234\rangle, \|1345\rangle, \|1256\rangle, \|1368\rangle, \|1237\rangle, \|1357\rangle, \|2346\rangle, \|3456\rangle, \|2367\rangle, \|3567\rangle\}$
4	$\hat{a}_3^\dagger\hat{a}_3 + \hat{a}_6^\dagger\hat{a}_6 + \hat{a}_8^\dagger\hat{a}_8 - \hat{a}_1^\dagger\hat{a}_1$	$\{\|1234\rangle, \|1238\rangle, \|1256\rangle, \|1247\rangle, \|1278\rangle, \|1356\rangle, \|1347\rangle, \|1378\rangle, \|1567\rangle\}$
5	$\hat{a}_4^\dagger\hat{a}_4 + \hat{a}_6^\dagger\hat{a}_6 + \hat{a}_7^\dagger\hat{a}_7 - \hat{a}_1^\dagger\hat{a}_7$	$\{\|1234\rangle, \|1236\rangle, \|1237\rangle, \|1245\rangle, \|1256\rangle, \|1257\rangle, \|1248\rangle, \|1268\rangle, \|1278\rangle\}$
6	$\hat{a}_4^\dagger\hat{a}_4 + \hat{a}_5^\dagger\hat{a}_5 + \hat{a}_8^\dagger\hat{a}_8 - \hat{a}_1^\dagger\hat{a}_1$	$\{\|1234\rangle, \|1256\rangle, \|1258\rangle, \|1267\rangle, \|1278\rangle, \|1345\rangle, \|1347\rangle, \|1567\rangle, \|1578\rangle\}$
7	$\hat{a}_4^\dagger\hat{a}_4 + \hat{a}_6^\dagger\hat{a}_6 + \hat{a}_8^\dagger\hat{a}_8 - \hat{a}_2^\dagger\hat{a}_2$	$\{\|1234\rangle, \|1245\rangle, \|1345\rangle, \|1236\rangle, \|1256\rangle, \|1356\rangle, \|1278\rangle, \|1378\rangle, \|1578\rangle\}$

possible N-electron configurations in $\wedge^N\mathcal{H}_r$. For each configuration $|s_k\rangle \in \mathcal{F}_{N,r}$, the first N natural orbitals are occupied and rest are unoccupied virtuals. $\mathcal{F}_{N,r}$ defines the full configuration interaction (FCI) ansatz that takes into account multi-reference (static) correlation between all configurations and dynamic correlation due to the concerted movement of electrons in a finite basis.

Ground-state wavefunctions that are *pinned* to the polytope boundary $\partial\mathcal{P}^1_{N,r}$ are eigenfunctions of at least one of the operators ${}^1\hat{O}_p \in B^1_{N,r}$ with eigenvalue zero. The boundary set of extremal 1-RDMs is defined by the set of operators ${}^1\hat{O}_p$ that *expose* the convex set $\mathcal{P}^1_{N,r}$ of pure N-representable 1-RDMs

$$\partial\mathcal{P}^1_p = \left\{ {}^1D \middle| \, \mathrm{Tr}({}^1\hat{O}_p\, {}^1D) = 0 \ \text{ for some } \ {}^1\hat{\mathrm{O}}_\mathrm{p} \in \mathrm{B}^1_{\mathrm{N,r}} \right\}. \tag{1.40}$$

This boundary set defines the set $\partial\mathcal{P}^1_p \subseteq \mathcal{F}_{N,r}$ of slater determinants that can contribute to the pth facet. Since operators ${}^1\hat{O}_p$ are diagonal, their expectation value for the N-fermion wavefunction ($|\Psi_N\rangle$) and the 1-RDM (${}^1D$) are equivalent, and pinned wavefunctions are pre-images of extremal 1-RDMs, i.e

$$\text{if } \ \langle\Psi_\mathrm{N}|{}^1\hat{\mathrm{O}}_\mathrm{p}|\Psi_\mathrm{N}\rangle \equiv \mathrm{Tr}\left({}^1\hat{\mathrm{O}}_\mathrm{p}\, {}^1\mathrm{D}\right) = 0 \tag{1.41}$$

$$\text{then } \ {}^1\mathrm{D} \equiv \binom{\mathrm{N}}{1} \mathrm{Tr}_{\mathrm{N}-1}\left(|\Psi_\mathrm{N}\rangle\langle\Psi_\mathrm{N}|\right) \in \partial\mathcal{P}^1_\mathrm{p}. \tag{1.42}$$

Table 1.3: A summary of spin selection rules for determinants pinned spectra in state spaces $\wedge^N\mathcal{H}_r$ with even r. While the total number of determinants contributing to the wavefunction ($\mathrm{N_{Total}} = \binom{\mathrm{r}}{\mathrm{N}}$) reduces to $\mathrm{N_{Spin}}$ for a given $\mathrm{M_z}$, pinned spectra can have contributions from fewer configurations. $\mathrm{N^*_{pin}} = \max_{\mathrm{p}}(\mathrm{N^p_{pin}})$ in the table is the maximum number of pinned determinants for a given state space and total spin $\mathrm{M_z}$.

State Space		Number of Determinants		
$\wedge^N\mathcal{H}_r$	$\langle \mathrm{S_z}\rangle$	$\mathrm{N_{Total}}$	$\mathrm{N_{Spin}}$	$\mathrm{N^*_{pin}}$
$\wedge^3\mathcal{H}_6$	$\frac{1}{2}$	20	9	3
	$\frac{3}{2}$		1	1
$\wedge^3\mathcal{H}_8$	$\frac{1}{2}$	56	24	24
	$\frac{3}{2}$		4	4
$\wedge^3\mathcal{H}_{10}$	$\frac{1}{2}$	120	50	30
	$\frac{3}{2}$		10	3
$\wedge^4\mathcal{H}_8$	0	70	36	10
	1		16	10
	2		1	1
$\wedge^4\mathcal{H}_{10}$	0	210	100	30
	1		50	30
	2		5	3
$\wedge^5\mathcal{H}_{10}$	$\frac{1}{2}$	252	100	40
	$\frac{3}{2}$		25	17
	$\frac{5}{2}$		1	1

For wavefunctions that are pinned to the boundary set $\partial\mathcal{P}^1$ the necessary and sufficient criterion for pure N-representability is met by the truncated ansatz ∂P^1_p and only those configurations $|s_k\rangle \in \partial\mathcal{P}^1_p$ may contribute to the pinned quantum state. The set exclusion $\mathcal{F}_{N,r} \setminus \partial\mathcal{P}^1_p$ comprises of configurations that may *not* contribute to a wavefunction pinned to facet p, giving rise to selection rules for slater determinants. Importantly, this necessary criterion for purity of an N-fermion quantum state is obtainable from single-party measurements.

Slater determinants $|s_k\rangle$ have each natural orbital either completely filled or empty with a spectrum of natural occupations that is given by the r-dimensional vector

$$\vec{s_k} = \sigma_k(1, 1, \cdots, 0, 0). \tag{1.43}$$

Each slater determinant $|s_k\rangle \in \partial P_p^1$ that contributes to extremal spectra must saturate the GPC operator ${}^1\hat{O}_p$. Additionally, the local spins of $\vec{m} = \{m_i, i = 1, \cdots, r\}$ of single particle orbitals must total the global spin M_z of the N-electron quantum state,

$$\vec{m}.\vec{s_k} = \langle S_z \rangle, \tag{1.44}$$

$$\kappa_{0,p} + \vec{\kappa_p}.\vec{s_k} = 0, \text{ and} \tag{1.45}$$

where $\vec{\kappa_p} = \left\{\kappa_{1,p}, \kappa_{2,p}, \cdots, \kappa_{r,p}\right\}$ is the vector of integer coefficients that define the affine inequality constraint ${}^1\hat{O}_p$ and $\vec{m}$ carries information about local spins on each orbital. Statements (1.45) and (1.44) form the basis of a spin selection rule for slater determinants for extremal spectra.

Table 1.2 lists determinants that constitute each pinned facet for singlet states ($M_z = 0$) in the state space $\wedge^4\mathcal{H}_8$, for which there are 14 GPCs that reduce to 7 unique constraints due to particle-hole symmetry outlined in [22]. The total number $\binom{8}{4}(= 70)$ possible determinants reduces to $\left(\binom{4}{2}\binom{4}{2}\right) = 36$ when one takes into account the total spin M_z. GPC facets $\{1, 2, 3\}$ are composed of 10 determinants that make up their pinned ansatz whereas facets $\{4, 5, 6, 7\}$ are constituted by 9 determinants each. The table lists boundary sets of slater determinants for each of the 7 unique facets, named by the canonical ordering of natural orbitals. A summary of spin selection rules for all even r state spaces for which the GPC are known is outlined in Table 1.3. In state space $\wedge^N\mathcal{H}_r$, the total number contributing determinants $\left(\mathrm{N_{Total}} = \binom{\mathrm{r}}{\mathrm{N}}\right)$ reduces to $\mathrm{N_{Spin}} = \left(\binom{\mathrm{r}_\alpha}{\mathrm{N}_\alpha}\binom{\mathrm{r}_\beta}{\mathrm{N}_\beta}\right)$ for a given total spin $\mathrm{M_z}$, and pinning to GPC facets further reduces the number of determinants that can contribute. In the Borland-Dennis setting ($N = 3, R = 6$), the total of 9 possible configurations reduce to 3 when one considers the generalized Pauli conditions. In state space $\wedge^3\mathcal{H}_8$ there is a single facet that encodes information about all the 24 possible determinants for doublet states.

There are multiple GPC facets in each state space and we report here the maximum

number of pinned determinants

$$\mathrm{N}^{*}_{\mathrm{Pin}} = \max_{{}^{1}\hat{\mathrm{O}}_{\mathrm{p}} \in \mathrm{B}^{1}_{\mathrm{N,r}}} (\mathrm{N}^{\mathrm{p}}_{\mathrm{Pin}}). \tag{1.46}$$

among all GPC facets for a given state space. In this way we obtain the minimum reduction in determinants ($\mathrm{N}_{\mathrm{Spin}} - \mathrm{N}^{*}_{\mathrm{Pin}}$) for pinned spectra. For instance, the ground state doublet ($M_z = \frac{1}{2}$) in $\wedge^5\mathcal{H}_{10}$ can have a-priori contributions from 100 different configurations. Since the maximum number of pinned determinants $\mathrm{N}^{*}_{\mathrm{pin}}$ to the GPCs facets in this state space is 40, pinning to GPCs obviates contribution from a minimum of 60 slater determinants. Similarly, consideration of GPCs results in savings of 26 determinants out of a total of 36 in $\wedge^4\mathcal{H}_8$, and 70 determinants out of a total of 100 in $\wedge^4\mathcal{H}_{10}$ for $M_z = 0$.

1.5 Correlated Energies from Extremal Occupation Spectra

The energy of an N-electron system can be written as a linear functional of its 2-electron reduced density matrix (2-RDM) [14],

$$E = \binom{N}{2} \mathrm{Tr}\,({}^{2}K\,{}^{2}D). \tag{1.47}$$

The reduced two-particle Hamiltonian ${}^{2}K$ encodes information about energetic relations between every particle-pair,

$${}^{2}K = \frac{1}{N-1}\left(\sum_{i=1}^{2} -\frac{1}{2}\bigtriangledown_i^2 - \left(\sum_{k}\frac{Z_{ik}}{r_{ik}}\right)\right) + \frac{1}{r_{12}}, \tag{1.48}$$

and the 2-RDM, that is obtained by integrating out all but two coordinates from the N-fermion density matrix,

$${}^{2}D(1,2;\bar{1},\bar{2}) = \int^{N} D(1,2,\cdots N;\bar{1},\bar{2},\cdots,N)d3\cdots dN, \tag{1.49}$$

gives the statistical dependance between all possible two-particle orbitals. Since electrons interact two at a time, the energy obtained in (1.47) is exact provided one is privy to conditions that ensure the 2-RDMs come from pure N-fermion quantum states (${}^2D \in \mathcal{P}^2$). Necessary conditions for pure N-representability of the 2-RDM have been proved by one of the authors [22], and extensive studies have confirmed that the variational minimization of energy over the ensemble representable set $\mathcal{E}^2$ of 2-RDMs gives chemical accuracy in the calculation of ground state energies [14, 24–34]. Since functional (1.47) is linear, the non-degenerate ground state invokes extremality conditions on the set $\mathcal{P}^2$ of pure N-representable 2-RDMs [12].

$$E_{gs} = \min_{{}^2D \in \mathcal{P}^2} \mathrm{Tr}({}^2K {}^2D), \text{ and,} \tag{1.50}$$

$${}^2D_{gs} \equiv \binom{N}{2} \mathrm{Tr}(|\Psi_{gs}\rangle\langle\Psi_{gs}|) \in \partial\mathcal{P}^2. \tag{1.51}$$

Variational minimization over the set $\mathcal{P}^2$ of pure N-representable 2-RDMs in (1.50) is then equivalent to diagonalizing the FCI Hamiltonian for finding the energy of a non-degenerate ground state, with the former yielding the 2-RDM, and the latter the wavefunction for the ground state. Necessary and sufficient conditions for pure N-representability of the 2-RDM have been elusive but, as outlined in the introduction, conditions on the 1-RDM that ensure that the wavefunction has at least one N-electron wavefunction as its pre-image are now known. Since the 1-RDM is obtained by integrating our coordinate 2 from the 2-RDM,

$${}^1D(1;\bar{1}) = \int^2 D(1,2;\bar{1},2)d2, \tag{1.52}$$

pinning of ground-state spectra to the boundary of the set of pure N-representable 1-RDMs is *sufficient* to ensure extremality of the 2-RDM, i.e,

$$\text{if } \binom{\mathrm{N}}{1} \mathrm{Tr}_{\mathrm{N}-1}(|\Psi_{\mathrm{gs}}\rangle\langle\Psi_{\mathrm{gs}}|) \in \partial\mathcal{P}^1 \tag{1.53}$$

$$\text{then } \binom{\mathrm{N}}{2} \mathrm{Tr}_{\mathrm{N}-2}(|\Psi_{\mathrm{gs}}\rangle\langle\Psi_{\mathrm{gs}}|) \in \partial\mathcal{P}^2. \tag{1.54}$$

The single-particle marginal is defined by the the polytope boundary $\partial\mathcal{P}^1$ that comprises of n_c hyperplanes in the space of $\mathbb{R}^r$ of natural orbital occupations for state space $\wedge^N\mathcal{H}_r$. The set of configurations that constitute each pinned facet p is given by (1.40). Diagonalization of the FCI Hamiltonian, analogous here to the variational minimization of the functional (1.47) over all configurations $|s_k\rangle \in \partial\mathcal{P}^1_p$, gives energy E_p for ground-state wavefunctions that saturate the pth boundary of the pure set $\mathcal{P}^1_{N,r}$. Minimizing the energy E_p obtained over all such facets $p \in [1, n_c]$ gives the optimal facet p^* and the best energetic approximation $|\Psi_{\partial\mathcal{P}^1_{p^*}}\rangle$ (referred to from here on as simply $|\Psi_{p^*}\rangle$) to $|\Psi_{gs}\rangle$ that can be reconstructed from knowledge of single-particle marginals.

$$\min(E_{\partial\mathcal{P}^1}) = \min_{{}^1D\in\partial\mathcal{P}^1} \mathrm{Tr}({}^2K^2D) \tag{1.55}$$

$$\text{such that } \ \mathrm{Tr}({}^1\hat{O}^1_pD) = 0. \tag{1.56}$$

Since the pinned ansatz for extremal 1-RDMs is a subset of the full-CI ansatz ($\partial\mathcal{P}^1_p \subseteq \mathcal{F}_{N,r}$), the energy of each pinned wavefunction is bounded from below by the Full-CI energy for the ground state ($E_p \geq E_{gs}$). The percentage correlation energy recovered from the set of extremal 1-RDMs on facet p is given by

$$(\%\ \mathrm{CE})_{\mathrm{p}} = \frac{\mathrm{E_p} - \mathrm{E_{HF}}}{\mathrm{E_{gs}} - \mathrm{E_{HF}}} \times 100, \tag{1.57}$$

where the Hartree-Fock energy E_{HF} is the energy due to the best single-determinant approximation of the N-body wavefunction. When a pinned facet contains only one determinant, the Hartree-Fock energy $E_{HF} \leq E_p$ and the value (1.57), may in principle, be negative.

Analytical and numerical investigation into the extent of saturation of pure set boundary $\partial\mathcal{P}^1$ [10, 12, 17–20, 35–39] has yielded consensus for their quasi-saturation for physical systems, now phenomenologically termed *quasipinning*. Furthermore, the reconstruction of quasipinned wavefunctions in terms of extremal 1-RDMs has very recently been proved to be energetically stable, i.e, the error in correlation energy (1.57) recovered from pinned ansatzes is bounded from above by the distance of quasipinned pure-state spectra from the pure set (polytope) boundary $\partial\mathcal{P}^1$ [39]. Constraints of the form (1.11) have been used recently in 1-RDM functional theories [40–42] and as initial guess in Lagrangian energy minimization [43]. With the optimization program (1.55), which gives the minimal energy facet for the boundary set of 1-RDMs $\partial\mathcal{P}^1$ in the basis of canonically ordered natural orbitals, we can probe the energetic proximity of quasipinned wavefunctions to their pinned approximations.

1.6 Sufficient Criterion for Openness

Conditions for pure N-representability given in section 1.2 are necessary and sufficient for the 1-RDM to have as its pre-image at least one N-fermion wavefunction. In Ref. [13] we have formalized the use of pure-state N-representability constraints (GPCs) to derive sufficient conditions for openness of an N-electron quantum system from sole knowledge of its occupation spectrum.

Theorem 1: For N electrons in r orbitals a diagonal, eigenvalue-ordered 1-RDM ${}^1D$, constrained to trace to N, is derivable from the integration of at least one *pure* N-electron density matrix (pure N-representable) if and if ${}^1D \in P^1_{(N,r)}$ where $P^1_{(N,r)}$ is the convex polytope whose facets are defined by Pauli and generalized Pauli conditions.

Proof: The proof is given by Klyachko in Ref. [9].

Similarly, the solution of the ensemble N-representability problem for the 1-RDM [6] can

be summarized as follows:

Theorem 2: For N electrons in r orbitals a diagonal, eigenvalue-ordered 1-RDMs ${}^1D$, constrained to trace to N, is derivable from the integration of at least one *ensemble* N-electron density matrix (ensemble N-representable) if and if ${}^1D \in E^1_{(N,r)}$ where $E^1_{(N,r)}$ is the convex polytope whose facets are defined by Pauli conditions.

Proof: The proof is given by Coleman in Ref. [6].

We present a corollary to these two theorems for open N-electron quantum systems. Because the N-representability of an RDM is invariant to unitary transformations of the orbitals, this corollary can be applied to an arbitrary non-diagonal 1-RDM by its unitary transformation to a diagonal eigenvalue-order 1-RDM [6]:

Corollary: If ${}^1D \in E^1_{(N,r)} \setminus P^1_{(N,r)}$, then the 1-RDM is only derivable by integration from an ensemble (open) N-electron density matrix.

Proof: The set inclusion ${}^1D \in E^1_{(N,r)} \setminus P^1_{(N,r)}$ implies from Theorems 1 and 2 that the 1-RDM is ensemble N-representable but not pure N-representable.

To use the generalized Pauli conditions to quantify a quantum system's interaction with its environment, we introduce a Euclidean metric δ to compute the shortest distance of a given set of orbital occupation numbers to the boundary of the convex polytope of pure N-representable occupation numbers. Occupation numbers are pure N-representable if and only if they represent at least one pure N-electron quantum system. We will refer to δ as the *pure distance*. For a system of 3 electrons in 6 orbitals we compute the δ by solving the

following constrained optimization by sequential quadratic programming [44]:

$$\begin{aligned} \delta(t) &= \sigma \min_{\vec{p}\in\mathbb{R}^6} ||\vec{n}-\vec{p}|| && (1.58)\\ \text{such that} \quad & p_{i+1} \leq p_i \text{ for all } i, && (1.59)\\ & \textstyle\sum_i p_i = 3, && (1.60)\\ & 0 \leq p_i \leq 1 \text{ for all } i, && (1.61)\\ & p_i + p_{7-i} = 1 \text{ for all } i, && (1.62)\\ & p_4 - p_5 - p_6 = 0. && (1.63) \end{aligned}$$

Eqs. (1.59) and (1.60) represent the ordering and trace conditions, respectively. Eq. (1.61) contains the Pauli exclusion principle for each of the occupation numbers. Finally, Eqs. (1.62) and (1.63) express the generalized Pauli conditions for a system of three electrons in six orbitals. $\mathbb{R}^6$ is the space of real vectors of length six. The symbol σ is chosen as either $+1$ or -1 to denote whether the distance to the boundary is from a set of occupation numbers *inside* the polytope or *outside* the polytope, respectively. While the metric above caters to the Borland Dennis setting, similar considerations of Generalized Pauli conditions for bigger system sizes can provide sufficient conditions for openness in N-fermion systems from knowledge of its 1-RDM. In Ref. [23], we have studied one such case where the structural simplicity afforded by an entangled p-qubit system allows an extension of Generalized Pauli conditions to p-qubits with arbitrarily large p.

1.7 Generalized Pauli Constraints for Qubits

If a system of N fermion particles and N fermion holes is restricted to N qubits, then the natural-orbital occupations, ordered from largest to smallest, obey the following sum rules

$$n_i + n_{(r+1)-i} = 1 \ \forall \ i \in \{1, 2, \cdots N\}. \tag{1.64}$$

Substitution of these restrictions into the generalized Pauli constraints for 3, 4, or 5 fermions, derived by Klyachko and Altunbulak, [9, 46] generates a single constraint corresponding to the constraint on 3, 4, or 5 qubits given by Higuchi et al. [45] For any number N of fermions, restricted to satisfy Eqs. (1.64), the generalized Pauli constraints are equivalent to the following single inequality constraint, derived by Higuchi et al. [45] for a network of N entangled qubits:

$$\left(\sum_{i=N+2}^{r} n_i \right) - n_{(N+1)} \geq 0. \tag{1.65}$$

For the three qubit system the Higuchi inequalities are of the form

$$n_5 + n_6 - n_4 \geq 0 \tag{1.66}$$

$$n_i + n_{7-i} = 1 \ \forall \ i \in \{1, 2, 3\} \tag{1.67}$$

which are just the Borland-Dennis constraints that ensure pure N-representability of three-electron states [8]. For the four-electron system there are 14 generalized Pauli inequalities [8, 9, 46], but with structural constraints in Eq. (1.64), we can reduce them to a single Higuchi condition

$$n_6 + n_7 + n_8 - n_5 \geq 0 \tag{1.68}$$

and the Pauli criteria. The generalized Pauli constraints increase in number and complexity with increasing system size. For 5 electrons in 10 spin orbitals (state space $\wedge^5 \mathcal{H}_{10}$) there are a total of 161 generalized Pauli constraints. When restricted by equalities (1.64), we have observed that the 161 constraints reduce to the single constraint for the 5-qubit system in Eq. (1.65). Identifying the hierarchical structure of significant constraints that apply to a general N-fermion pure state has been the focus of recent work [38, 47]; furthermore, enumerating the general Pauli constraints for larger systems ($N \geq 5$) is ongoing [48]. Violation of the inequalities in Eq. (1.65) ensures that electron occupations can only come

from a mixed (ensemble) state with the nature and the extent of this violation serving to quantify correlation and entanglement in many-electron quantum domains [12, 13].

1.8 References

[1] W. Pauli, Zeit. Phys. A **31**, 765 (1925), ISSN 0044-3328, URL http://dx.doi.org/10.1007/BF02980631.

[2] E. C. Stoner, Philosophical Magazine Series 6 **48**, 719 (1924), URL http://www.tandfonline.com/doi/abs/10.1080/14786442408634535.

[3] P. A. M. Dirac, Proceedings of the Royal Society of London. Series A **112**, 661 (1926), URL http://rspa.royalsocietypublishing.org/content/112/762/661.short.

[4] W. Heisenberg, Z. Phys. A Hadrons Nuclei **38**, 411 (1926), ISSN 0044-3328, URL http://dx.doi.org/10.1007/BF01397160.

[5] J. Von Neumann, *Mathematical foundations of quantum mechanics*, 2 (Princeton university press, 1955).

[6] A. J. Coleman, Rev. Mod. Phys. **35**, 668 (1963), URL http://link.aps.org/doi/10.1103/RevModPhys.35.668.

[7] D. W. Smith, Phys. Rev. **147**, 896 (1966), URL http://link.aps.org/doi/10.1103/PhysRev.147.896.

[8] R. E. Borland and K. Dennis, J. Phys. B **5**, 7 (1972), URL http://stacks.iop.org/0022-3700/5/i=1/a=009.

[9] A. A. Klyachko, J. Phys. Conf. Ser. **36**, 72 (2006), URL http://stacks.iop.org/1742-6596/36/i=1/a=014.

[10] C. Schilling, D. Gross, and M. Christandl, Phys. Rev. Lett. **110**, 040404 (2013), URL http://link.aps.org/doi/10.1103/PhysRevLett.110.040404.

[11] C. L. Benavides-Riveros, J. M. Gracia-Bondía, and M. Springborg, Phys. Rev. A **88**, 022508 (2013), URL http://link.aps.org/doi/10.1103/PhysRevA.88.022508.

[12] R. Chakraborty and D. A. Mazziotti, Phys. Rev. A **89**, 042505 (2014), URL http://link.aps.org/doi/10.1103/PhysRevA.89.042505.

[13] R. Chakraborty and D. A. Mazziotti, Phys. Rev. A **91**, 010101 (2015), URL http://link.aps.org/doi/10.1103/PhysRevA.91.010101.

[14] D. A. Mazziotti, Phys. Rev. Lett. **108**, 263002 (2012), URL http://link.aps.org/doi/10.1103/PhysRevLett.108.263002.

[15] A. J. Coleman and V. I. Yukalov, *Reduced Density Matrices: Coulson's Challenge* (Springer-Verlag, New York, 2000).

[16] M. B. Ruskai, Journal of Physics A: Mathematical and Theoretical **40**, F961 (2007).

[17] R. Chakraborty and D. A. Mazziotti, International Journal of Quantum Chemistry **115**, 1305 (2015), ISSN 1097-461X, URL http://dx.doi.org/10.1002/qua.24934.

[18] C. Schilling, Physical Review B **92**, 155149 (2015).

[19] F. Tennie, D. Ebler, V. Vedral, and C. Schilling, Phys. Rev. A **93**, 042126 (2016), URL https://link.aps.org/doi/10.1103/PhysRevA.93.042126.

[20] F. Tennie, D. Ebler, V. Vedral, and C. Schilling, Phys. Rev. A **93**, 042126 (2016), URL http://link.aps.org/doi/10.1103/PhysRevA.93.042126.

[21] R. Chakraborty and D. A. Mazziotti, International Journal of Quantum Chemistry **116**, 784 (2016), ISSN 1097-461X, URL http://dx.doi.org/10.1002/qua.25120.

[22] D. A. Mazziotti, Physical Review A **94**, 032516 (2016).

[23] R. Chakraborty and D. A. Mazziotti, The Journal of Chemical Physics **146**, 184101 (2017), http://dx.doi.org/10.1063/1.4982927, URL http://dx.doi.org/10.1063/1.4982927.

[24] C. Garrod and J. K. Percus, J. Math. Phys. **5**, 1756 (1964), URL http://scitation.aip.org/content/aip/journal/jmp/5/12/10.1063/1.1704098.

[25] M. Nakata, H. Nakatsuji, M. Ehara, M. Fukuda, K. Nakata, and K. Fujisawa, J. Chem. Phys **114**, 8282 (2001), URL http://scitation.aip.org/content/aip/journal/jcp/114/19/10.1063/1.1360199.

[26] D. A. Mazziotti, Phys. Rev. A **65**, 062511 (2002), URL http://link.aps.org/doi/10.1103/PhysRevA.65.062511.

[27] A. E. Rothman and D. A. Mazziotti, Phys. Rev. A **78**, 032510 (2008), URL http://link.aps.org/doi/10.1103/PhysRevA.78.032510.

[28] J. R. Hammond and D. A. Mazziotti, Phys. Rev. A **73**, 062505 (2006), URL http://link.aps.org/doi/10.1103/PhysRevA.73.062505.

[29] M. Nakata, B. J. Braams, K. Fujisawa, M. Fukuda, J. K. Percus, M. Yamashita, and Z. Zhao, J. Chem. Phys **128**, 164113 (2008), URL http://scitation.aip.org/content/aip/journal/jcp/128/16/10.1063/1.2911696.

[30] B. Verstichel, H. van Aggelen, D. Van Neck, P. W. Ayers, and P. Bultinck, Phys. Rev. A **80**, 032508 (2009), URL http://link.aps.org/doi/10.1103/PhysRevA.80.032508.

[31] N. Shenvi and A. F. Izmaylov, Phys. Rev. Lett. **105**, 213003 (2010), URL http://link.aps.org/doi/10.1103/PhysRevLett.105.213003.

[32] K. Pelzer, L. Greenman, G. Gidofalvi, and D. A. Mazziotti, J. Phys. Chem. A **115**, 5632 (2011), URL http://dx.doi.org/10.1021/jp2017192.

[33] B. Verstichel, H. van Aggelen, W. Poelmans, and D. Van Neck, Phys. Rev. Lett. **108**, 213001 (2012), URL http://link.aps.org/doi/10.1103/PhysRevLett.108.213001.

[34] D. A. Mazziotti, Chemical Reviews **112**, 244 (2012), pMID: 21863900, http://dx.doi.org/10.1021/cr2000493, URL http://dx.doi.org/10.1021/cr2000493.

[35] C. L. Benavides-Riveros and M. Springborg, Phys. Rev. A **92**, 012512 (2015), URL http://link.aps.org/doi/10.1103/PhysRevA.92.012512.

[36] C. L. Benavides-Riveros and M. Springborg, Physical Review A **92**, 012512 (2015).

[37] C. Schilling, Phys. Rev. A **91**, 022105 (2015), URL http://link.aps.org/doi/10.1103/PhysRevA.91.022105.

[38] C. Schilling, Ph.D. thesis, Johannes Gutenberg-Universität Mainz (2014).

[39] C. Schilling, C. L. Benavides-Riveros, and P. Vrana, arXiv preprint arXiv:1703.01612 (2017).

[40] M. Piris, J. Chem. Phys. **141**, 044107 (2014), URL http://scitation.aip.org/content/aip/journal/jcp/141/4/10.1063/1.4890653.

[41] M. Piris, J. M. Matxain, and X. Lopez, J. Chem. Phys. **139**, 234109 (2013), URL http://scitation.aip.org/content/aip/journal/jcp/139/23/10.1063/1.4844075.

[42] M. Piris, J. M. Matxain, X. Lopez, and J. M. Ugalde, J. Chem. Phys **132**, 031103 (2010), URL http://scitation.aip.org/content/aip/journal/jcp/132/3/10.1063/1.3298694.

[43] Y. Wang, J. Wang, and H. Lischka, International Journal of Quantum Chemistry (2017).

[44] P. Gill, W. Murray, and M. Saunders, SIOPT **12**, 979 (2002), URL http://dx.doi.org/10.1137/S1052623499350013.

[45] A. Higuchi, A. Sudbery, and J. Szulc, Phys. Rev. Lett. **90**, 107902 (2003), URL http://link.aps.org/doi/10.1103/PhysRevLett.90.107902.

[46] M. Altunbulak and A. Klyachko, Comm. Math. Phys. **282**, 287 (2008), ISSN 0010-3616, URL http://dx.doi.org/10.1007/s00220-008-0552-z.

[47] F. Tennie, V. Vedral, and C. Schilling, arXiv preprint arXiv:1509.00358 (2015).

[48] M. Altunbulak, Ph.D. thesis, bilkent university (2008).

CHAPTER 2

APPLICATIONS

This chapter contains excerpts from the following published articles:

- Reproduced from [R. Chakraborty and D. A. Mazziotti, *Phys. Rev. A*, **89**, 042505 (2014)]. Copyright 2014, American Physical Society.
- Reproduced from [R. Chakraborty and D. A. Mazziotti, *Phys. Rev. A*, **91**, 010101 (2015)]. Copyright 2015, American Physical Society.
- Reproduced from [R. Chakraborty and D. A. Mazziotti, *Int. J. Quantum Chem.*, **116**, 784 (2016)]. Copyright 2016, John Wiley and Sons.
- Reproduced from [R. Chakraborty and D. A. Mazziotti, *J. Chem. Phys.*, **146**, 184101 (2017)]. Copyright 2017, American Institute of Physics.

2.1 Methodogy

Selection rules (summarized in table 1.3) that enforce the generalized Pauli exclusion principle were employed to enumerate slater determinants that contribute to each facet for all even r state spaces for which 1-RDM pure N-representability conditions are known. GPCs number 31 in $\wedge^3\mathcal{H}_8$, 103 in $\wedge^3\mathcal{H}_{10}$, 14 in $\wedge^4\mathcal{H}_8$, 125 in $\wedge^4\mathcal{H}_{10}$ and 161 in $\wedge^5\mathcal{H}_{10}$ [1]. Using particle-hole symmetry, we were able to calculate pure N-representability constraints for state spaces $\wedge^{r-N}\mathcal{H}_r$ provided GPCs for $\wedge^N\mathcal{H}_r$ were known [2]. A program that calculates the ground state energy of an N-electron system for the FCI ansatz and for truncated ansatzes for pinned approximations to the wavefunction for all facets ${}^1\hat{O}_p \in B^1_{N,r}$ was written in Maple [3]. Diagonalization of the configuration interaction Hamiltonian was carried out with a QR decomposition code with numerical precision of upto 50 places of decimal. Optimization program (1.55) gave the minimal energy facet p^* for each species for a given state space, taking into account the entire polytope boundary $\partial\mathcal{P}^1$. Euclidean distance to

boundaries of the pure set was calculated using optimization algorithms described in detail in [4] with sequential quadratic programs that were seeded with a random initial guess. The software package GAMESS [5, 6] was used to evaluate two-electron integrals and to compute Hartree-Fock orbitals and their energies.

For each atom or molecule the 1-RDM's spectrum of occupation numbers was obtained by computing the wave function from a full configuration interaction (FCI) calculation in arbitrary-precision floating-point arithmetic. For comparison the 1-RDMs of several four-electron molecules were also computed without the wave function from the variational 2-RDM method with approximate ensemble N-representability conditions on the 2-RDM [7–9]. The pure, ensemble and Slater distances were calculated in arbitrary-precision arithmetic by the constrained optimizations described in section 1.3.2. Unless otherwise specified, all molecules were treated in the Slater-type-orbital (STO-3G) basis set in which each Slater function is expanded in three Gaussian functions [10]. The number r of orbitals is always set to be twice the number N of electrons. To achieve either $N = 3$ and $N = 4$ with $2N$ orbitals, we froze core and virtual orbitals in atoms and molecules, as needed. Equilibrium geometries were obtained from the *Computational Chemistry Comparison and Benchmark Database* [11].

The following sections summarize computational results compiled from previous work [4, 12–14]. In Ref. [4], we assessed constraint saturation by 1-RDM spectra for ground and excited states of atoms and molecules with the consideration of time-reversal symmetry for even N systems. Excited state spectra, and the nature of their pinning to the generalized Pauli conditions, were investigated in Ref. [13]. Pinned approximations to wavefunctions that are quasipinned allowed us to capture correlation energies from extremal occupations (see Ref. [15]). Violation of generalized Pauli conditions give sufficient conditions for openness in a many-electron quantum system from sole knowledge of its 1-RDM. In Ref. [12], and in Ref. [14] we have formulated a kinematic viewpoint for noise-assisted energy transfer in photosynthetic light harvesting in terms of the set expansion of one-electron reduced density

matrices.

2.2 Pinning in Atoms and Molecules

We evaluate the deviation of the 1-RDM spectrum in atoms and molecules from the boundary of the ensemble N-representable 1-RDM set and boundaries of the pure N-representable 1-RDM sets both with and without time-reversal symmetry.

2.2.1 Lithium

For the three-electron lithium atom the Euclidean distances of the 1-RDM's spectrum to the pure and ensemble boundaries and the nearest Slater point were computed. Previous calculations on the lithium atom were inconclusive about whether the 1-RDM's spectrum was pinned or only nearly pinned (quasi-pinned) to one of the generalized Pauli constraints [16]. To resolve the issue, we performed both the FCI and the Euclidean-distance calculations with high-precision floating-point arithmetic *with as many as 35 digits of precision.* Table 2.1 shows the pure and Slater distances as functions of the floating-point precision. While the Slater distance remains constant at 8.53×10^{-5} as the precision is increased, the logarithm of the pure distance decreases linearly with the precision (also refer to Fig. 2.1). These results demonstrate within the limit of numerical precision that *the ground-state 1-RDM spectrum for the lithium atom is pinned to the boundary of the pure set.*

Table 2.2 shows the Euclidean distances of ground- and excited-state 1-RDM spectra of the lithium atom from the pure and ensemble boundaries and from the Slater point. Calculations of the 1-RDMs and the Euclidean distances were performed with a numerical precision of thirty decimals. While the spectra of the ground states of a given spin symmetry were always found to be pinned to the boundary of the pure set, *the spectra of the excited states were not necessarily pinned.* For example, the spectrum of excited state 3 lies well within the boundary of the pure set. The difference in pinning between the ground and

Table 2.1: For the ground state of lithium the pure and Slater distances of the 1-RDM spectrum of natural occupation numbers are shown as functions of the floating-point precision. While the Slater distance remains constant at 8.53×10^{-5} as the floating-point precision is increased, the logarithm of the pure distance decreases linearly with the precision. These results demonstrate that the ground-state 1-RDM spectrum of lithium is pinned to the boundary of the pure set.

Precision	Pure	Slater
5	1e-05	8.00e-05
10	1e-10	8.53e-05
15	1e-15	8.53e-05
20	1e-20	8.53e-05
25	1e-25	8.53e-05
30	1e-30	8.53e-05
35	1e-35	8.53e-05

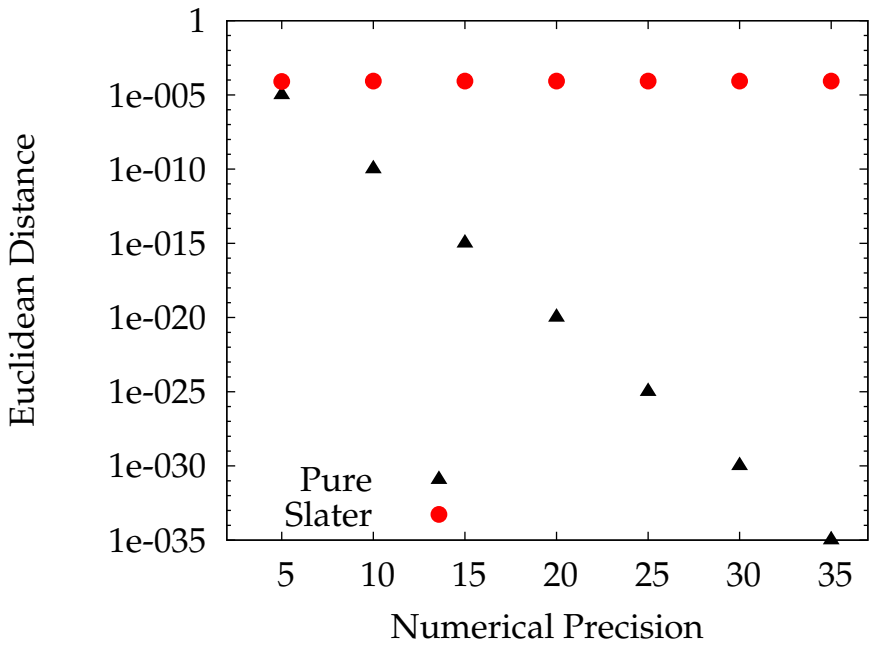

Figure 2.1: For the ground state of the lithium atom the logarithm of the pure distance decreases linearly with the precision of the floating-point calculations. The plot demonstrates that the ground-state 1-RDM spectrum of lithium is pinned to a facet to at least 35 digits of floating-point precision.

excited states was foreshadowed by the discussion in section 1.3.1 of the necessary 2-RDM condition for pinning. A 1-RDM spectrum can be pinned to a facet of the generalized Pauli

Table 2.2: For the ground and excited states of the lithium atom, Euclidean distances of the 1-RDM spectra from the pure and ensemble boundaries and from the Slater point are shown. While the spectra of the ground states of a given spin symmetry were always found to be pinned to the boundary of the pure set, the spectra of the excited states were not necessarily pinned. For example, the spectrum of excited state 3 lies well within the boundary of the pure set. Calculations of the 1-RDMs and the Euclidean distances were performed with a numerical precision of thirty decimals.

			Euclidean distance		
State	S_z	Energy (a.u)	Pure	Ensemble	Slater
0	0.5	-7.316	1.00e-30	1.00e-30	8.53e-05
1		-7.230	1.00e-30	4.10e-05	1.41e-04
2		-5.264	1.00e-30	1.00e-30	1.75e-01
3		-5.244	2.72e-01	3.65e-01	8.16e-01
4	1.5	-5.244	1.00e-30	1.00e-30	1.00e-30

condition only if the 2-RDM is pinned to the boundary of the pure N-representable 2-RDM set. While a ground-state 2-RDM is always on the boundaries of the ensemble and the pure N-representable sets of 2-RDMs, an excited-state 2-RDM is not necessarily on the boundary of either the ensemble or pure sets. Hence, the spectrum of an excited-state 1-RDM is not necessarily on the boundary of the pure set of N-representable 1-RDMs.

2.2.2 Strongly correlated systems

The neutral triatomic hydrogen molecule is strongly correlated due to multi-reference effects that arise due to degeneracy in electronic configurations [17, 18]. The spectrum of the ground-state 1-RDM, we find, is on the boundary of the pure set for all molecular geometries. This constitutes the first numerical evidence of pinning of the 1-RDM spectra in a strongly correlated molecule. Table 2.7 gives a summary of the results for linear and triangular geometries of H_3. The spectra of the excited-state 1-RDMs are not necessarily on the boundary of the pure set, as demonstrated for both molecular geometries by state 2. As functions of the bond angle in ground-state H_3, (a) the Hartree-Fock and correlation energies as well as (b) the minimum Euclidean distances to the boundaries of the pure and ensemble

Table 2.3: Euclidean distances to the pure and ensemble boundaries and the Slater point for linear and equilateral configurations of neutral triatomic hydrogen H_3. The spectrum of the ground-state 1-RDM, we find, is on the boundary of the pure set for both molecular geometries. The spectra of the excited-state 1-RDMs are not necessarily on the boundary of the pure set, as demonstrated for both molecular geometries by state 2. The distance to the nearest Slater point, which represents a completely uncorrelated system, shows that the H_3 is significantly correlated, especially in the vicinity of the equilateral geometry.

				Occupation numbers			Euclidean distance		
Configuration	State	S_z	Energy(a.u)	λ_1	λ_2	λ_3	Pure	Ensemble	Slater
Linear	0	0.5	-2.958	0.9902	0.9789	0.9691	1.0e-30	1.1e-02	5.5e-02
	1		-2.666	1.0000	0.6479	0.6479	1.0e-30	1.0e-30	7.0e-01
	2		-2.448	0.6667	0.6667	0.6667	2.7e-01	3.7e-01	8.2e-01
	3		-2.358	1.0000	0.6530	0.6530	1.0e-30	1.0e-30	6.9e-01
	4	1.5	-2.448	1.0000	1.0000	1.0000	1.0e-30	1.0e-30	1.0e-30
Equilateral	0	0.5	-3.308	0.9929	0.9909	0.9838	1.0e-30	7.7e-03	2.8e-02
	1		-3.304	1.0000	0.9835	0.9835	1.0e-30	1.0e-30	3.3e-02
	2		-2.652	0.6667	0.6667	0.6667	2.7e-01	3.7e-01	8.2e-01
	3		-2.368	1.0000	0.5182	0.5182	1.0e-30	1.0e-30	9.6e-01
	4	1.5	-2.652	1.0000	1.0000	1.0000	1.0e-30	1.0e-30	1.0e-30

sets and the nearest Slater point are shown in Fig. 2.2. Both the ensemble and Slater distances are greater than 0.01 for all bond angles while the pure distance is zero for all angles. The large distance to the nearest Slater point shows that H_3 is significantly correlated. The vanishing pure distance shows that the generalized Pauli conditions can be saturated even when the traditional Pauli conditions are far from being saturated.

Euclidean distances of the 1-RDM spectra to the boundaries of pure (Smith), pure (Klyachko), and ensemble (Pauli) sets and the Slater point are shown in Table 2.4 for the ground states of several four-electron molecules in eight spin orbitals ($\wedge^4[\mathcal{H}_8]$). Because the ground-state 1-RDM spectra in all cases are pairwise degenerate, they are pinned to the boundary of the Smith set. The Euclidean distances of the 1-RDM spectra to the pure (Klyachko) and ensemble (Pauli) boundaries are found to be the same in all cases. The pure (Klyachko) distances are nonzero because the generalized Pauli conditions describing the boundary of the Klyachko polytope break time-reversal symmetry.

The rectangular H_4 molecule, comprised of two H_2 monomers, has well-documented multi-reference correlations effects in the form of pronounced diradical character [19]. As

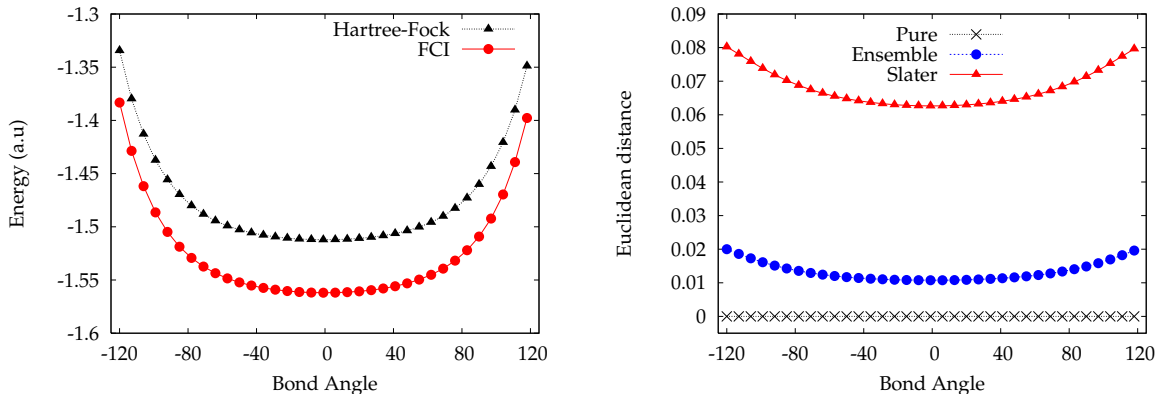

(a) Potential energy surface (b) Euclidean distance

Figure 2.2: As functions of the bond angle in H_3, (a) the Hartree-Fock and correlation energies as well as (b) the minimum Euclidean distances to the boundaries of the pure and ensemble sets and the nearest Slater point are shown. Both the ensemble and Slater distances in (b) are greater than 0.01 for all bond angles while the pure distance is zero for all angles. The large distance to the nearest Slater point shows that H_3 is significantly correlated. The vanishing pure distance shows that the generalized Pauli conditions can be saturated even when the traditional Pauli conditions are far from being saturated.

Table 2.4: Euclidean distances of the 1-RDM spectra to pure (Smith), pure (Klyachko), and ensemble (Pauli) sets and the Slater point are shown for the ground states of several four-electron molecules. Because the ground-state 1-RDM spectra in all cases are pairwise degenerate, they are pinned to the boundary of the Smith set. The Euclidean distances of the 1-RDM spectra to the pure (Klyachko) and ensemble (Pauli) boundaries are the same in all cases. The pure (Klyachko) distances are nonzero because the generalized Pauli conditions describing the boundary of the Klyachko polytope break time-reversal symmetry. All molecules except H_4 are treated in their equilibrium geometries from the Computational Chemistry Comparison and Benchmark Database [11]. The H_4 molecule is treated with the four hydrogen atoms in a square with sides of 1.058 Å.

Molecule	Occupation numbers				Pure		Ensemble	Slater
	$\lambda_1 = \lambda_2$	$\lambda_3 = \lambda_4$	$\lambda_5 = \lambda_6$	$\lambda_7 = \lambda_8$	Smith	Klyachko		
LiH	1.0000	0.9985	0.0013	0.0002	0.00000	0.00002	0.00002	0.00281
BH	0.9991	0.9260	0.0375	0.0375	0.00000	0.00098	0.00098	0.12876
BeH_2	0.9957	0.9938	0.0068	0.0037	0.00000	0.00398	0.00398	0.01527
H_4	0.9694	0.5000	0.5000	0.0306	0.00000	0.03270	0.03270	1.00187

functions of distance between H_2 dimers, Fig. 2.3 shows (a) the potential energy surfaces from FCI and the variational 2-RDM method as well as (b) the minimum Euclidean distances from the 1-RDM spectra to the ensemble set and a Slater point from FCI and the variational 2-RDM method. The peak in the Slater distance at a dimer distance of 1 Å shows that the

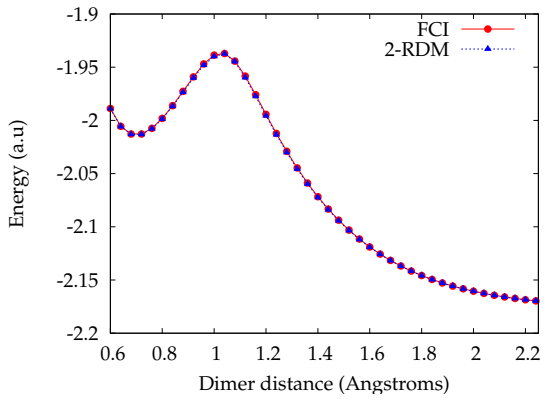

(a) Potential energy surface

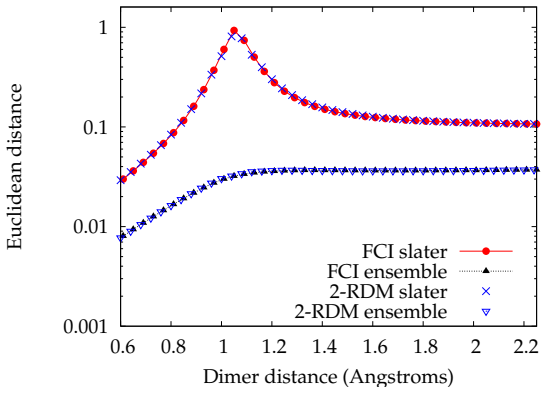

(b) Euclidean distance

Figure 2.3: As functions of the distance between H_2 dimers, the figure shows (a) the potential energy surfaces from FCI and the variational 2-RDM method as well as (b) the minimum Euclidean distances from the 1-RDM spectra to the ensemble set and a Slater point from FCI and the variational 2-RDM method. The peak in the Slater distance at a dimer distance of 1 Å shows that the maximum electron correlation occurs when the two H_2 dimers form a square H_4 molecule. While the ensemble distance is about 0.01 or larger for all dimer distances, the 1-RDM spectra are pinned to Smith's set of pure N-representable 1-RDMs with time-reversal symmetry. The figures also show that the FCI and variational 2-RDM methods give similar results for both energies and Euclidean distances.

maximum electron correlation occurs when the two H_2 dimers form a square diradical H_4 molecule. While the ensemble distance is about 0.01 or larger for all dimer distances, the 1-RDM spectra are pinned to Smith's set of pure N-representable 1-RDMs with time-reversal symmetry. The figures also show that the FCI and variational 2-RDM methods give similar results for both energies and Euclidean distances.

2.3 Excited States

We explore the proximity of the 1-RDM to the boundaries of the sets for excited states in three-and four-electron atoms and molecules, the five-electron cyclopentadienyl radical, and the seven-electron Fenna-Matthews-Olson complex.

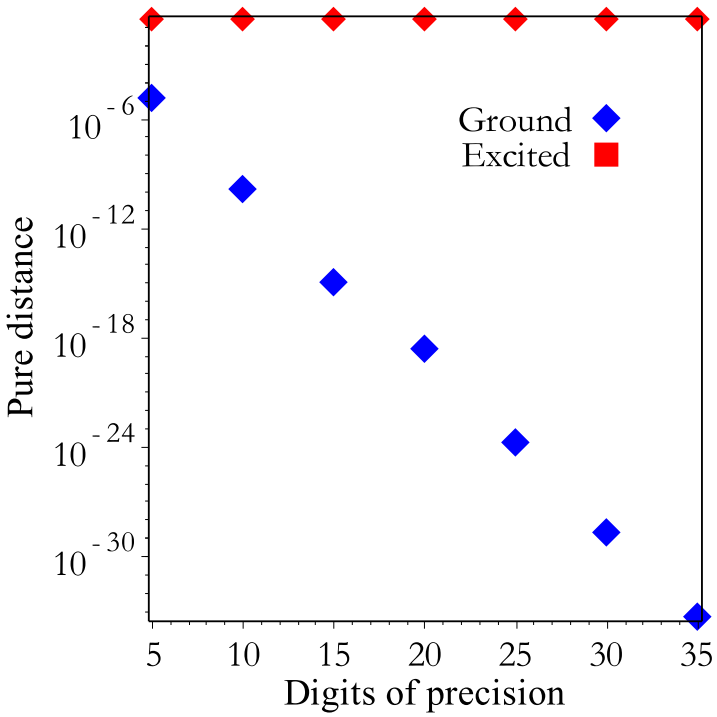

Figure 2.4: Pure distances for the ground and excited states of Lithium ($^2S_{1/2}$). The excited state 1-RDM, unlike the ground state, is not pinned to generalized Pauli conditions.

2.3.1 Atoms and Molecules

For the ground and excited states of the lithium atom the Euclidean distances of the 1-RDM's natural occupation numbers to the pure and ensemble boundaries and the nearest Slater point were computed [4]. The occupation numbers in this calculation, as well as all other calculations, were obtained by computing the 1-RDM from the wave function of a full configuration interaction calculation in a Slater-type orbital basis set with three Gaussians (STO-3G) [10]. Figure 2.4 shows the pure distances for the ground- and excited-state 1-RDMs as functions of floating-point precision. These two states have energies of -7.32 a.u. and -5.24 a.u., respectively. While the logarithm of pure distance for the ground state decreases linearly with the precision, pure distance for the excited state remains constant at 2.71 x 10^{-1} as floating-point precision of the occupation numbers and the computed distances is increased. These results demonstrate that while the ground-state 1-RDM of three-electron atoms and molecules have been consistently pinned to the generalized Pauli conditions to

35-or-more digits using arbitrary floating-point precision [4], the excited-state 1-RDMs of three-electron atoms and molecules are not necessarily pinned to these conditions. The excited-state 1-RDMs of 3-electron atoms and molecules can lie within the convex polytope described by the generalized Pauli conditions. In another 3-electron example, the ground-state 1-RDM of the strongly correlated H_3 molecule is pinned to the pure set as shown in table 2.5 [4]. The first excited-state 1-RDM like the ground-state 1-RDM is also pinned to the boundary, but the 1-RDM of state 3 lies a considerable distance from the facets of the pure set.

By Smith's theorem, for systems with time reversal symmetry, pairwise degeneracy of natural occupations is sufficient, although not necessary, for pure N-representability [20]. Because the *generalized Pauli conditions define facets that break time-reversal symmetry*, they define a pure set of 1-RDMs that is larger than the set of evenly degenerate 1-RDMs [4]. In closed-shell species like LiH, BeH_2 and H_4 we observe that the spectra of ground-state occupation numbers are *quasi-pinned*, which is to say are close but not exactly on the boundary of the pure set. For the ground states of these molecules where the natural occupation numbers are pairwise degenerate the generalized Pauli conditions reduce to the usual Pauli exclusion principle, and hence, the pure and ensemble distances are equal [4]. Excited states which unpair the electrons break the time-reversal symmetry, opening again the possibility for pinning. In fact, the first excited states (labeled state 1) of LiH, BeH_2 and H_4 with spin symmetry $S_z = 1.0$ in the STO-3G basis set are pinned to generalized Pauli conditions. Pure distances for excited states 2 and 3, shown in table 2.5, reveal that these states are not pinned. The pure distance for some excited states like state 2 of BeH_2 (pure distance of 0.0349) and states 2 and 3 for H_4 (pure distances of 0.04901 and 0.22301, respectively) show considerable deviation from the generalized Pauli conditions. The variety of pinning, quasi-pinning, and non-pinning of excited-state 1-RDM spectra reflects the structural complexity of excited states, which can be highly correlated and entangled.

Table 2.5: For the ground and excited states of H_3, LiH, BeH_2, and H_4 the Euclidean distances of the 1-RDM's natural occupation numbers to the pure and ensemble boundaries and the nearest Slater point are reported. While the Slater distances are nonzero in all cases, reflecting the presence of electron correlation, the pure distances are zero for the ground-state of H_3 as well as for the first excited states of H_3, LiH, BeH_2, and H_4. Other higher-in-energy excited states are far from pinned, showcasing the range of pinning (or non-pinning) that is possible.

Molecule	State	Energy (a.u)	Spin (S_z)	Euclidean distance		
				Pure	Ensemble	Slater
H_3 (triangular)	0	-3.308	0.5	0.00000	0.00775	0.02817
	1	-3.304	0.5	0.00000	0.00000	0.03296
	2	-2.652	0.5	0.27217	0.36515	0.81650
LiH ($^1\Sigma$)	0	-8.855	0.0	0.00002	0.00002	0.00281
	1	-8.714	1.0	0.00000	0.00000	0.00007
	2	-8.701	0.0	0.00003	0.00003	0.77307
	3	-8.678	0.0	0.00004	0.00004	1.00000
BeH_2 ($^1\Sigma_g$)	0	-15.565	0.0	0.00009	0.00009	0.01147
	1	-15.286	1.0	0.00000	0.00000	0.00653
	2	-15.286	0.0	0.00349	0.00349	1.00002
	3	-15.260	0.0	0.00035	0.00035	1.00000
H_4 (square)	0	-4.654	0.0	0.03226	0.03226	0.91365
	1	-4.636	1.0	0.00000	0.00337	0.07488
	2	-4.502	0.0	0.04901	0.04901	0.91990
	3	-4.279	1.0	0.22301	0.22301	0.78672

2.3.2 Cyclopentadienyl Radical

The cyclopentadienyl is a symmetric five-membered radical subject to Jahn-Teller distortion. Here we consider the correlation of the 5 π electrons in the 10 π spin orbitals spanning the space $\wedge^5\mathcal{H}_{10}$. We computed the ground- and three excited-state wave functions with doublet spin symmetry $\langle\hat{S}_z\rangle = 0.5$ from full configuration interaction calculations in the basis of Slater determinants from a ground-state multi-configuration self-consistent field calculation. Calculations for the cyclopentadienyl radical were carried out in the Dunning-type Correlation Consistent basis set (cc-pVDZ).

For each state Figure 2.5 shows the Euclidean distance to each facet of the 1-RDM

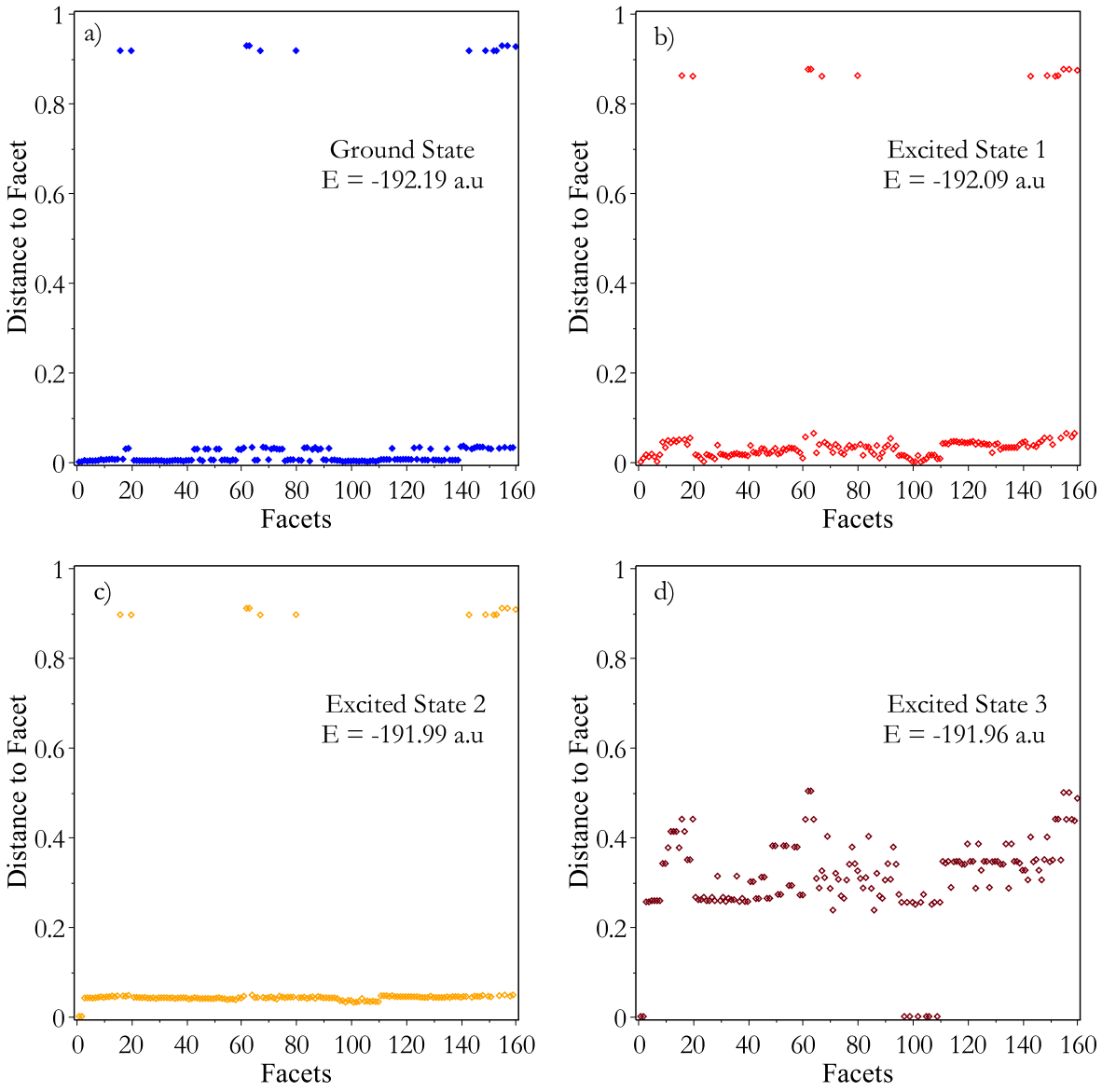

Figure 2.5: The Euclidean distance to each facet of the 1-RDM set is shown for the following doublet states: (a) ground state, (b) first excited state, (c) second excited state, and (d) third excited state. We find that the ground-state 1-RDM *is not exactly pinned* to any of the generalized Pauli conditions. The ground state and the first two excited states have 1-RDMs that are far from a selected number of facets to which the Euclidean distances greater than 0.8. In contrast, the third excited state's 1-RDM does not have any facets further than 0.6 even though it is farther than 0.2 from most of its facets except a small number clustered around 0 and 100.

set generated by a generalized Pauli condition. We find that the ground-state 1-RDM is not exactly pinned to any of the generalized Pauli conditions. Likely, the exact pinning

of the 1-RDM to the generalized Pauli conditions in the case of three-electron atoms and molecules like Li and H_3 is special to the case of three electrons in six orbitals where the quantum system does not have many degrees of freedom. Similarly, the three excited states of the cyclopentadienyl radical also do not exhibit exact pinning of the 1-RDM to any of the generalized Pauli conditions. Nevertheless, the comparison of the four graphs in Fig. 2.5, which serve as fingerprints for each of the states in terms of the generalized Pauli conditions, reveals qualitative differences. For example, the ground state and the first two excited states have 1-RDMs that are far from a select number of facets to which the Euclidean distances are greater than 0.8. In contrast, the third excited state's 1-RDM does not have any facets farther than 0.6 even though it is farther than 0.2 from most of its facets except a small number of nearly pinned facets clustered around 0 and 100.

The differences between the lowest three states and the third excited state reveal that it is important to consider the distances to all of the facets from the generalized Pauli conditions to construct a complete fingerprint from the information available in these conditions. This conclusion is especially true for $N \geq 5$ where the number of facets becomes quite large. For the ground state and the three excited states Table 2.6 reports not only the minimum distance to a facet of the pure 1-RDM set (pure distance) but also the harmonic, geometric, and arithmetic means of the Euclidean distances to each facet of the set. While the harmonic mean is similar to the minimum distance, the geometric and arithmetic means provide information about the distance to the majority of facets. For example, while the harmonic-mean distance and the minimum distance are smallest for the ground state, the first and the third excited state, the geometric- and arithmetic-mean distances are largest for the third excited state, reflecting that its 1-RDM is far from the majority of the generalized Pauli facets.

2.3.3 FMO complex

The Fenna-Matthews-Olson (FMO) complex in green-sulfur bacteria consists of three parts, each with seven chromophores embedded in a protein matrix. As in previous work [9, 21–25],

Table 2.6: The minimum distance to a facet of the pure 1-RDM set (pure distance) as well as the harmonic, geometric, and arithmetic means of the Euclidean distances to each facet are reported for the doublet ground state and the first three doublet excited states. While the harmonic mean is similar to the minimum distance, the geometric and arithmetic means provide information about the distance to the majority of facets. For example, while the harmonic-mean distance and the minimum distance are smallest for the ground state and the third excited state, the geometric- and arithmetic-mean distances are largest for the third excited state.

			Means of Pure distance				
Molecule	State		Harmonic	Geometric	Arithmetic	Std dev.	Minimum
$C_5H_5^{\cdot}$	Ground		0.0037	0.0103	0.0907	0.2566	0.0001
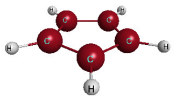	Excited	1	0.0044	0.0303	0.1014	0.2366	0.0001
$^2B_1$, C_{2v}		2	0.0206	0.0516	0.1157	0.2425	0.0005
		3	0.0023	0.2178	0.3119	0.0952	0.0001

we model the seven chromophores as a single-electron two-level system. Due to environmental differences, each of the seven chromophores has a slightly different energy. If we restrict the model to the single-excitation manifold, then the Hamiltonian is a 7×7 matrix where have been determined from computational and experimental data [22, 24]. Diagonalization of the Hamiltonian generates seven stationary excited-state wave functions. Each 1-RDM is readily computed from contraction of its corresponding wave function. While the generalized Pauli conditions have not been previously applied to a 7-electron quantum system, for a two-level excitonic system the conditions significantly simplify to a single generalized Pauli condition (or facet) [26].

Table 2.7 shows the minimum distances to the pure, ensemble, and Slater boundaries for the ground and excited states of the seven-site FMO complex. Because the ground state in this model is a Slater determinant, its Slater, ensemble, and pure distances vanish. In contrast, the Slater distances of all seven excited states are nonzero (≥ 0.85), reflecting the presence of electron correlation. The ensemble distances of all seven excited states are also nonzero, indicating that the 1-RDMs of these states do not lie on the ensemble boundary. The pure distances, however, for all the excited states except states 3 and 6 are zero to arbitrary

Table 2.7: Minimum distances to the pure, ensemble, and Slater boundaries for the ground and excited states of the seven-site FMO complex are shown. Because the ground state in this model is a Slater determinant, its Slater, ensemble, and pure distances vanish. In contrast, the Slater distances of all seven excited states are nonzero (≥ 0.85), reflecting the presence of electron correlation. The ensemble distances of all seven excited states are also nonzero. The pure distances, however, for all the excited states except states 3 and 6 are zero to arbitrary digits of precision.

			Euclidean distances		
FMO	State	Energy (cm^{-1})	Pure	Ensemble	Slater
Ground	0	0.00	0.0000	0.0000	0.0000
Excited	1	-23.74	0.0000	0.0005	0.8876
	2	101.97	0.0000	0.0048	0.8528
	3	120.96	0.0020	0.0085	0.9958
	4	268.37	0.0000	0.0141	0.9246
	5	307.13	0.0000	0.0001	0.9320
	6	332.00	0.0003	0.0003	0.9784
	7	513.32	0.0000	0.0003	0.8797

digits of precision. States 3 and 6 have the greatest Slater distances, indicating that they have the highest level of electron correlation of the seven excited states. Interestingly, state 3 is nearly degenerate with state 2, and states 6 is nearly degenerate with state 5. States 3 and 6 have the higher energies in these energetically quasi-degenerate pairs. Pinning to the generalized Pauli conditions in the FMO complex gives a glimpse into the structural complexity of excited state 1-RDMs which can either be pinned, quasi-pinned, or buried deep inside the pure set.

While the ground state 2-RDM is always on the boundary of the ensemble N-representable set of 2-RDM, excited-state 2-RDMs can lie on the boundary or inside the ensemble N-representable set [4]. The ability of excited state 2-RDMs to lie inside the set reflects the potential of excited states to exhibit even greater complexity in their electron correlation than ground states. The location of the 2-RDM in it N-representable set also imposes constraints on the position of the 1-RDM in its set. For example, as we previously showed [4], the 2-RDM lying on (or near) the boundary of its pure set is a necessary condition for the 1-RDM to lie on (or near) the boundary of its set, that is for the 1-RDM to be pinned

(or quasi-pinned) to a generalized Pauli condition. Consequently, the 1-RDMs of excited states can be expected to exhibit a range of behaviors including pinned, quasi-pinned. and unpinned.

Although the ground-state 1-RDM in three-electron systems in six orbitals is pinned to the generalized Pauli conditions, the excited-state 1-RDMs of these systems are not necessarily pinned. At least one of the excited-state 1-RDMs of H_3 is pinned to the boundary of the set, but other excited-state 1-RDMs of H_3 lie significantly within the set. We also presented some of the first calculations of the generalized Pauli conditions for five-electron molecules in 10 orbitals. We found that neither the ground- state 1-RDM nor any of the excited-state 1-RDMs of the five-electron cyclopentadienyl radical is exactly pinned to the generalized Pauli conditions. While further calculations are necessary, this result indicates that the pinning of the ground-state 1-RDM in three-electron systems is likely the exception rather than the rule due to the small number of quantum degrees of freedom in three-electron systems in six orbitals. Nevertheless, for the ground and excited states of the cyclopentadienyl radical the spectrum of Euclidean distances to each facet provides a unique identifier of the state. Comparison of the spectra of distances between states reveals important information about the similarities and differences between states. For example, we observe that the third is excited state is significantly different from either the ground state or the first two excited states.

Molecular systems with even numbers of electrons are special in that their 1-RDMs can be made pure N-representable by selecting the natural occupation numbers to be pairwise degenerate which enforces time-reversal symmetry [20]. Because the generalized Pauli conditions break time-reversal symmetry, the 1-RDMs from four-electron singlet states are not pinned to the generalized Pauli conditions. However, these systems can be excited to non-singlet states that break the time-reversal symmetry. We found, in particular, that the first excited states of several four-electron molecules have 1-RDMs that are pinned to the generalized Pauli conditions. Other higher-lying states are not pinned to these conditions.

Table 2.8: Table enumerates pinned ansatzes and their correlation energy recovery due to 5 minimal energy facets for the ground state $N_2^+(D_{\infty h}, A_g)$ in state space $\wedge^5\mathcal{H}_{10}$.

p	Coefficients ($\vec{\kappa}_p$)	Pinned Ansatz (∂P_p^1)	%CE
1	$\{15,-7,-7,3,3,-7,-7,3,3,13,3\}$	$\{\|12345\rangle, \|12457\rangle, \|12578\rangle, \|12367\rangle, \|12468\rangle, \|13568\rangle, \|14567\rangle\}$	92.41
2	$\{15,-7,-7,-7,3,3,3,3,-7,13,3\}$	$\{\|12345\rangle, \|12578\rangle, \|12367\rangle, \|12468\rangle, \|13568\rangle\}$	89.01
3	$\{15,-3,-3,-3,-3,-3,-13,7,7,7,7\}$	$\{\|12345\rangle, \|12367\rangle, \|12468\rangle, \|13568\rangle, \|14567\rangle\}$	85.65
4	$\{15,-7,-7,3,-7,3,3,-7,3,13,3\}$	$\{\|12345\rangle, \|12578\rangle, \|12367\rangle, \|12468\rangle, \|14567\rangle\}$	84.82
5	$\{15,-7,-7,-7,3,3,-7,13,3,3,3\}$	$\{\|12345\rangle, \|12367\rangle, \|12468\rangle, \|13568\rangle, \|2369(10)\rangle\}$	83.54

Therefore, the four-electron systems manifest a full range of potential behaviors from pinning and quasi-pinning to non-pinning.

A seven-electron model of the Fenna-Matthews-Olson complex in green-sulfur bacteria was also examined with respect to the generalized Pauli conditions. While the ground state of the model is a Slater determinant by definition, each of the seven excited states exhibits nontrivial correlation with a non-vanishing Slater distance. Furthermore, none of the excited states is pinned to the boundary of the ensemble N-representable set of 1-RDMs, and yet five of the seven excited states are exactly pinned to the pure N-representable set of 1-RDMs. The two states that do not exhibit pinning also show the greatest degree of electron correlation as measured by the Slater distance. These results for the FMO complex as well as the results for the three-, four-, and five-electron atoms and molecules highlight the important information contained in the generalized Pauli conditions as well as demonstrate their applicability to understanding the structure and correlation of both ground and excited states.

2.4 Correlation Energies from Extremal Occupations

In this section, we apply our formalism for the reconstruction of quantum states from extremal occupation spectra to the atomic isoelectronic sequence of boron, dissociation pathways in hydrogen chains, and in conjugated π electrons in cyclic planar ring systems that display (non, anti- and) aromatic behaviour.

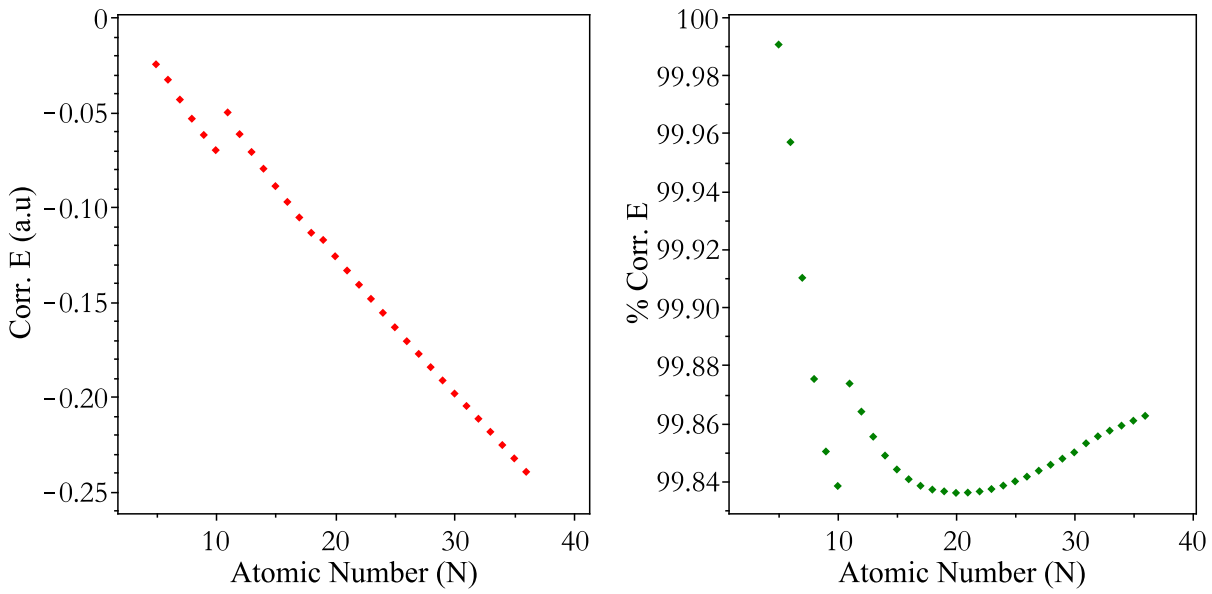

Figure 2.6: Correlation energy recovered by GPCs in $\wedge^5\mathcal{H}_{10}$ for the boron isoelectronic sequence in the 6-31G basis. GPCs recover between $[99.84\%, 99.99\%]$ of the correlation energy from B to Kr^{31+}. The slight kink in the curves are due to screening effect of the d shell added to Na^{+6} in the third period.

2.4.1 Atoms and Diatomics

Knowledge of pure N-representability conditions in $\wedge^5\mathcal{H}_{10}$ allows correlation energy capture beyond the Hartree-Fock limit in the boron isoelectronic sequence (figure 2.6). Absolute value of correlation energy decreases steadily down the sequence as electrons become less correlated on being more tightly held by the increased nuclear charge (left). The percentage correlation energy recovered (right) shows improvement due to GPCs over the Hartree-Fock limit, which lies in the range $[99.84\%, 99.99\%]$ for all atoms between B and Kr^{31+} in the second, third and fourth periods of the periodic table. Calculations reported her were performed in the split valence 6-31G basis, which explains the slight kink in the curves for correlation energies recovered as extra shells are added, starting with Na^{+6} in the third period.

Electron correlation plays a major role in determining the equilibrium geometry of the the dinitrogen molecule that shares three pairs of electrons between the two nitrogens [27]. The singly charged cation N_2^+ has bond order $\frac{5}{2}$, sharing 5 electrons between the two nitrogen

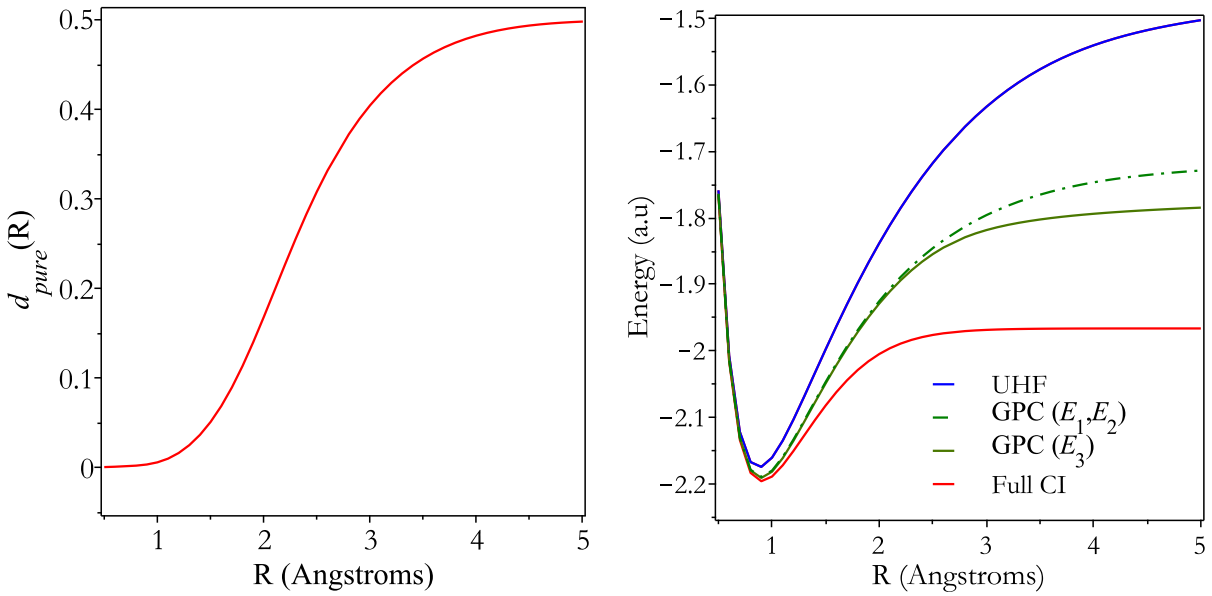

Figure 2.7: Dissociation curve for the linear hydrogen chain H_4 shows correlation energy recovered by GPC facets $\{E_1, E_2, E_3\}$ in green that are bounded from above by the Hartree-Fock energy (blue) and from below by the FCI curve in red.

atoms. Correlation energy of N_2^+ in its equilibrium geometry was calculated to be -0.083 a.u in the minimal STO-3G basis. Table 2.8 enumerates pinned ansatzes and their correlation energy recovery for the 5 minimal energy facets for the ground state of $N_2^+(D_{\infty h}, A_g)$ in state space $\wedge^5\mathcal{H}_{10}$. The full-CI ansatz has 13 determinants which reduces to 7 for the minimal energy GPC facet p^*. The best pinned approximation to the wavefunction is able to recover 92.41% of the correlation energy and the 4 other facets, that have similar structure in terms of the integer coefficients $\vec{\kappa}_p$ but comprise of fewer (five) determinants are able to recover between 89.01% and 83.54% of the correlation energy.

2.4.2 Hydrogen Chains

The dissociation pathway of linear hydrogen chains involves multi-reference effects as the polymer becomes maximally entangled in the dissociative limit due to interchangeable spins of electrons on each hydrogen [28]. Strong correlation in the linear hydrogen tetramer H_4 is evident in the correlation energy that increases almost 60-fold from -0.0078 a.u at 0.5 Å to

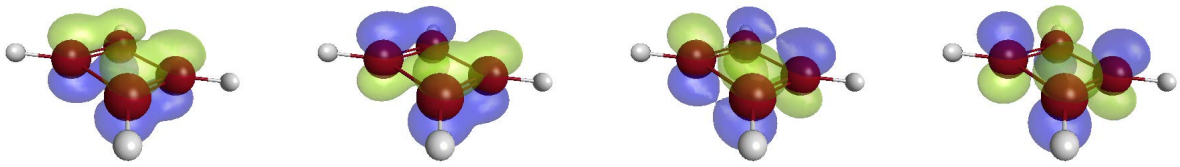

Figure 2.8: Natural Orbitals in the π-space of ground state cyclobutadiene ($C_4H_4, D_{2h},^1 A_g$).

-0.4633 a.u at 5.0 Å. Figure 2.7 shows minimum distance to the boundaries of the pure set (left) and the energy recovered by GPC facets (right) comparing them to the FCI and the unrestricted Hartree-Fock (UHF) Energies. Ordering of facets is as per table 1.2 and facets $1, 2$ and 3 are reminiscent of the Higuchi inequality [26] for 4-qubit systems (see also table 1.2), each of which allow a priori contribution from 10 out of a total of 36 determinants allowed for the ground state singlet. GPC facets 1 and 3 are isoenergetic and reproduce qualitatively the dissociative process, while being bounded from below by the full-CI energy and from above by the Hartree-Fock energy. The pure distance increases as the system becomes more entangled, reaching its maximum value $\frac{1}{2}$ in the dissociative limit. GPC facets capture correlation energy above and beyond the Hartree-Fock limit even in the limit of dissociation, facet (the curve E_3) giving the best energetic approximation to the FCI wavefunction.

2.4.3 Conjugated π Systems

Planar systems with conjugated π electrons constitute strongly correlated electronic quantum domains that exhibit non-, anti- and aromatic behavior. Table 2.9 lists GPC saturation and correlation energy recovered by minimal energy facets for the ionization sequences for cyclic conjugated π systems. The cyclopropenyl cation ($C_3H_3^+, (C_{2v},^1 A_1)$) is the smallest compound that exhibits aromatic behavior with 2 π electrons in a conjugated trigonal planar ring. For two electrons in six spin orbitals ($\wedge^2\mathcal{H}_4$), pairwise degeneracy of orbital occupations

Table 2.9: Table shows correlation energies recovered by the optimal pinned ansatz for ionization sequences of conjugated cyclic hydrocarbons that display non-, anti- and aromatic behavior.

Species	State Space	Number of	Facet	CE	%CE
	$\wedge^N\mathcal{H}_r$	Determinants	Distance	(a.u)	
$C_3H_3^+$	$\wedge^2\mathcal{H}_6$	3 (3)	0.00000	-0.02735	100.00
$C_3H_3^{\cdot}$	$\wedge^3\mathcal{H}_6$	3 (3)	0.00000	-0.04550	100.00
$C_3H_3^-$	$\wedge^4\mathcal{H}_6$	3 (3)	0.00000	-0.04209	100.00
$C_4H_4^+$	$\wedge^3\mathcal{H}_8$	6 (6)	0.00000	-0.04054	100.00
C_4H_4	$\wedge^4\mathcal{H}_8$	6 (12)	0.09999	-0.09664	57.06
$C_4H_4^-$	$\wedge^5\mathcal{H}_8$	10 (10)	0.00000	-0.04381	100.00
$C_5H_5^{2+}$	$\wedge^3\mathcal{H}_{10}$	13 (24)	0.00120	-0.05364	98.18
$C_5H_5^+$	$\wedge^4\mathcal{H}_{10}$	16 (52)	0.03587	-0.08447	61.23
$C_5H_5^{\cdot}$	$\wedge^5\mathcal{H}_{10}$	11 (48)	0.05656	-0.09642	55.71
$C_5H_5^-$	$\wedge^6\mathcal{H}_{10}$	22 (52)	0.04502	-0.07171	52.23
$C_5H_5^{2-}$	$\wedge^7\mathcal{H}_{10}$	13 (24)	0.00102	-0.05059	97.84

is necessary and sufficient to ensure pure N-representability of the 1-RDM [20] and the spectrum is pinned to GPC boundaries. Ground state of the free radical $C_3H_3^{\cdot}$ is pinned to Borland-Dennis constraints in the state space $\wedge^3\mathcal{H}_6$. Due to conditions (1.53) and (1.54) all of the correlation energy (100%) is recovered for pinned spectra for which $d_{pure} = 0$. The anion $C_3H_3^-$, on the other hand is similarly pinned to the Smith constraints. Figure 2.8 shows the CI natural orbitals of the anti aromatic π system in the cyclobutadiene. GPCs are able to recover only 57% of the correlation energy of the strongly correlated neutral C_4H_4 with a correlation energy of -0.09664 a.u. For even N systems, while pairwise degeneracy of occupations ensures pure N-representability of the 1-RDMs, GPCs due to Klyachko [29, 30] contain 1-RDMs that break time reversal symmetry of the Hamiltonian, a property that could be useful in the study of these species in the presence of a magnetic field. Both the cyclobutadienyl cation and anion ($C_4H_4^+, C_4H_4^-$) are pinned to GPC boundaries in state spaces $\wedge^3\mathcal{H}_8$ and $\wedge^5\mathcal{H}_8$, recovering all of the correlation energy. The ionization sequence of the cyclopentadienyl radical highlights the potential of GPCs in simplifying the electronic structure of correlated molecules by reducing the number of configurations that contribute to pinned approximations of a quasi-pinned wavefunction. The ionization sequence of $C_5H_5^{\cdot}$

has each of the species quasipinned. While the optimal facet is able to recover 98.18% and 61.23% of the correlation energy in the doubly and singly charged cation, the pinned ansatz for the free radical recovers 55.71%. Optimal facets for quasipinned anions $C_5H_5^-$ and $C_5H_5^{2-}$ were found to recover 52.23% and 97.84% of the correlation energy. The table shows an interesting trend of being less pinned (and hence recovering a smaller percentage of the correlation energy) on approaching half-filling. The number of configurations for a many-electron quantum system are maximum at half-filling and for the strongly entangled π system in our example, boundary set 1-RDMs are not able to capture all correlation effects and one needs to resort to higher p-RDMs to recover entanglement in the system.

2.5 Open Quantum Systems

Correlation and entanglement play a key role in the energy transfer dynamics of excitons. For many-electron systems, the exciton is entangled not only with electrons within a single molecule or moiety [9], but also with molecular complexes in different spatial domains [19, 19, 21, 22]. Our simple model for the entangled many-electron system has N electrons, each with access to states ground and excited. When limited to its intrinsic (spin) degree of freedom, excitations in electrons can be viewed as spin states that couple to an external magnetic field like in qubits. While there are $2N$ spin orbitals in the system the wavefunction may have contributions from an exponentially scaling number (2^N) of slater determinants. We first look at the three chromophore subsystem of the Fenna-Matthews-Olson (FMO) complex which has been shown to have a quantum efficiency similar to that of the full seven chromophore network [24]. We are then able to extend our formalism to study noise and entanglement in the full 7-chromophore network using generalized Pauli constraints for qubits.

In light harvesting antennae complexes such as the Fenna-Matthews-Olson (FMO) complex, the excitation is channelled towards the reaction center (sink) when entangled chromophores begin to interact with the surrounding protein matrix [23, 31]. The FMO is

comprised of three monomers, each consisting of a seven chromophore network, which serve as light harvesting antennae in green sulphur bacteria. The Hamiltonian for the system is given by a 7×7 matrix derived from previous work by Adolphs and Renger [32] that is given by:

$$\hat{H} = \sum_{j=1}^{M} \hbar\omega_j \sigma_j^+ \sigma_j^- + \sum_{j \neq l} \hbar v_{j,l} (\sigma_j^- \sigma_l^+ + \sigma_j^+ \sigma_l^-), \tag{2.1}$$

where σ_j^+ (σ_j^-) creates (annihilates) a single excitation on chromophore j. The site energy of each chromophore is $\hbar\omega_j$ while the coupling constant between the pair of chromophores j and l is $\hbar v_{j,l}$. The form of our Hamiltonian, as in Ref. (CM15), restricts the system to the manifold of single excitations.

The time evolution of the system's density matrix is governed by the *quantum Liouville equation*

$$\frac{d}{dt} D = -\frac{i}{\hbar} [\hat{H}, D] + \hat{L}(D) \tag{2.2}$$

where D is the density matrix

$$D = \sum_{k,l} \rho_l^k |\Psi_k\rangle\langle\Psi_l|, \tag{2.3}$$

ρ_l^k are the elements of the density matrix D in the basis set of wavefunctions $\{\Psi_k\}$, representing an excitation on the k^{th} chromophore,, and $\hat{L}$ is the Lindblad operator, which accounts for interactions of the $M \leq 7$ chromophores with the environment. The Lindblad operator is chosen as the sum of three operators that account for dephasing, dissipation, and loss to the reaction center (sink)

$$\hat{L}(D) = \hat{L}_{\text{deph}}(D) + \hat{L}_{\text{diss}}(D) + \hat{L}_{\text{sink}}(D) \tag{2.4}$$

where

$$\hat{L}_{\text{deph}}(D) = \alpha \sum_k 2\langle k|D|k\rangle |k\rangle\langle k| - \{|k\rangle\langle k|, D\}, \tag{2.5}$$

$$\hat{L}_{\text{diss}}(D) = \beta \sum_k 2\langle k|D|k\rangle |g\rangle\langle g| - \{|k\rangle\langle k|, D\}, \tag{2.6}$$

$$\hat{L}_{\text{sink}}(D) = 2\gamma\langle 3|D|3\rangle |s\rangle\langle s| - \gamma\{|3\rangle\langle 3|, D\}. \tag{2.7}$$

The $|g\rangle$ denotes the state in which each of the M chromophores is in its ground state, the $|k\rangle$ represent the M excited states with each state having a single excitation on one of the M chromophores, the state $|s\rangle$ denotes the reaction center (sink), and $|3\rangle$ indicates the excited state of the third chromophore multiplied by the ground states of the other $M-1$ chromophores.

The model incorporates two types of noise that affect the energy transfer. First, dissipation transfers energy from the chromophores back into the environment, wasting that energy. Second, dephasing dampens the coherence within the chromophore system. Finally, the Lindblad operator $\hat{L}_{\text{sink}}(D)$ is responsible for transferring energy from the third chromophore into reaction center, which acts as an energy sink and becomes site 8 in the density matrix. Details of the Lindbladian formalism for the $M \leq 7$ chromophore network can be found in the appendix and in refs. [9, 12, 24]. Unless otherwise noted, the rate parameters in the Lindblad operators for dephasing (α), dissipation (β), and the sink (γ) are chosen to be 7.26×10^{-5}, 1.21×10^{-8} and 1.52×10^{-4} a.u respectively in atomic units of inverse time. The protein matrix that surrounds the chromophore network in the FMO interacts with it through dispersion forces that arise from instantaneous dipole-dipole interactions. Phonon modes of the bath couple to the chromophore network and the system has finite-temperature effects at physiological temperatures. All these environmental influences can be modeled in the Lindbladian formalism. Although the Linbladian operators are Markovian in time, non-Markovian effects will not significantly affect the results presented here on the relationship between the violation of the generalized Pauli constraints from quantum noise and energy

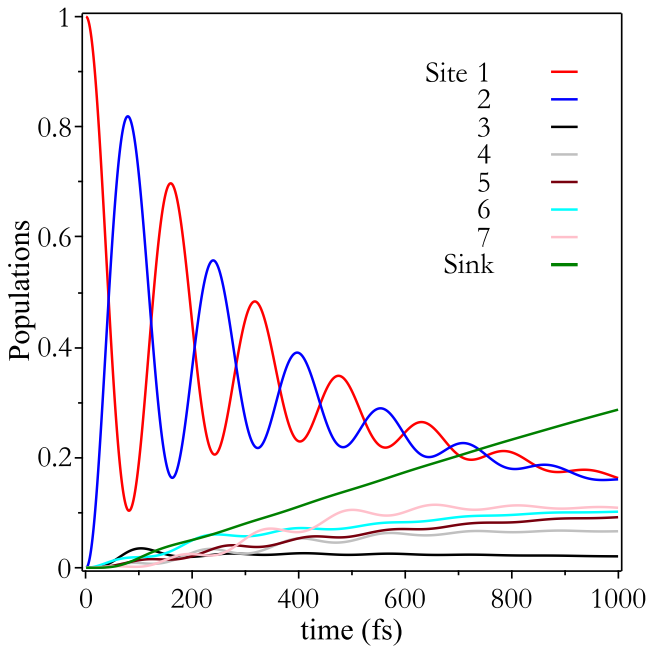

Figure 2.9: Site and sink populations in the FMO. Coherence lifetime between chromophores in is of the order of 1 ps after which the system relaxes back to its ground state as the excitation leaves the network having transferred energy to the reaction center.

transfer in quantum systems.

As an incident photon excites an electron on site 1, a delocalized exciton oscillates between sites, interacts with the surroundings, and finally reaches the reaction center where light reactions commence. Fig. 2.9 shows with femtosecond resolution the site and sink population in the FMO for the duration of 1 ps. The excitation initially bounces back and forth between sites 1 and 2 but with the combination of entanglement between chromophores in the network and noise on coupling with the surrounding proteins it finds a way to the sink whose population (shown by the curve in green) gradually increases. Coherence lifetime between chromophores in is of the order of 1 ps after which the system relaxes back to its ground state as the excitation leaves the network.

Table 2.10: The 1-electron and N-electron indicators of environmental effects, the pure distance $\delta(t)$ and the idempotency criterion $\gamma(t)$, are shown in the presence and the absence of environmental interactions. In the presence of environmental effects the system becomes open (ensemble) for $t > 0$ which is reflected in both the *nonzero* idempotency $\gamma(t)$ and the *negative* pure distance $\delta(t)$.

	Idempotency criterion $\gamma(t)$		Pure distance $\delta(t)$	
Time (fs)	No Bath	Bath	No Bath	Bath
0	1×10^{-15}	0.0000	1×10^{-15}	0.0000
100	1×10^{-15}	0.3777	1×10^{-15}	-0.0231
200	1×10^{-15}	0.5408	1×10^{-15}	-0.0695
300	1×10^{-15}	0.6107	1×10^{-15}	-0.1139
400	1×10^{-15}	0.6405	1×10^{-15}	-0.1515
500	1×10^{-15}	0.6603	1×10^{-15}	-0.1454
1000	1×10^{-15}	0.6712	1×10^{-15}	-0.0072
10000	1×10^{-15}	0.0089	1×10^{-15}	0.0003

2.5.1 Noise and Transport

The degree to which the system interacts with its environment can be examined from the idempotency of the N-electron (exciton) exciton density matrix:

$$\gamma(t) = \left[\mathrm{Tr}(^{N}D(t)) - \mathrm{Tr}(^{N}D(t)^{2}) \right]. \tag{2.8}$$

The $\gamma(t)$ is nonzero if and only if the quantum system is open. While $\gamma(t)$ provides a definitive answer to whether the system is open, it requires knowledge of the N-electron (exciton) density matrix. The N-electron density matrix can be readily computed for some model quantum systems, but its cost for many realistic quantum systems scales exponentially with system size.

Table 1 shows the 1-electron and N-electron indicators of environmental effects, the pure distance $\delta(t)$ and the idempotency criterion $\gamma(t)$, in the presence and the absence of environmental interactions. At $t = 0$, just after the first chromophore is excited, the three-chromophore network is in a pure (closed) state. In the absence of environmental effects the system remains inside the pure set for all time t. In fact, its spectrum of occupation

numbers lies on the boundary of the set except when strong correlation due to degeneracy in the populations of sites 1 and 2 pushes the occupation spectrum inside the set. In the presence of environmental effects the system becomes open (ensemble) for $t > 0$ which is reflected in both the *nonzero* idempotency $\gamma(t)$ and the *negative* pure distance $\delta(t)$. At 500 fs, for example, the idempotency γ is positive with a value of 0.6603 and the pure distance δ is negative with a value of -0.1454. By 10 ps, when the N-electron density matrix begins to regain idempotency with γ decreasing to 0.0089, δ shows that the spectrum of natural occupation numbers reenters the polytope of pure 1-RDMs with $\delta = 0.0003$. Importantly, δ can be positive for nonzero γ because the negative pure distance δ is a sufficient but not a necessary condition for openness.

Figure 2.10 compares the pure distance $\delta(t)$ as a time-dependent indicator of the openness of a quantum system for both closed (no bath) and open (with bath) quantum systems for times in the range 0-3 ps. In the closed system the pure distance is always nonnegative, and in the open system the pure distance is frequently negative. An important feature of Fig. 2.10 is that positive spikes in pure distance, representing the movement of occupation numbers inside the polytope, occur at times when the entanglement between sites 1 and 2 is maximal. This coincidence demonstrates the interplay between openness and entanglement [33, 34]. The openness of quantum systems (namely, its interaction with the environment) is typically evident in the occupation numbers of the 1-RDM, but when a quantum system is strongly entangled, the evidence of openness in the 1-RDM disappears. Higher RDMs are required in such cases to obtain a certificate for the openness of the system. Systems with greater entanglement between homogeneous components, previous results indicate, require greater environmental noise for maximal efficiency [35]. The present results indicate that in systems that are strongly correlated or entangled greater noise is required to force the 1-RDM to explore the larger set of occupation numbers associated with open quantum systems.

The system's trajectory in population space (the space of natural occupation numbers) provides a dynamical map of quantum information as it flows though the system, which

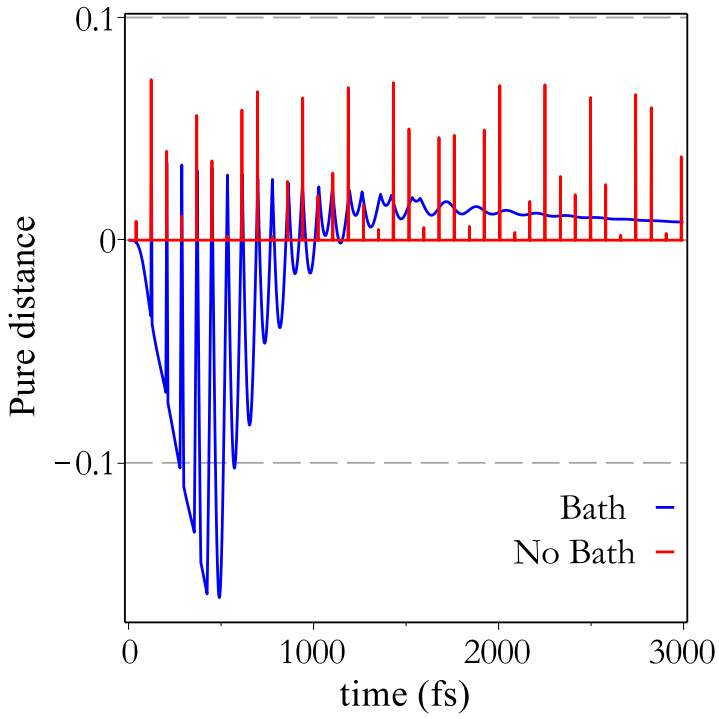

Figure 2.10: The pure distance $\delta(t)$ is compared for closed and open quantum systems for a time range of 0-3 ps. In the closed system the pure distance is always nonnegative, and in the open system the pure distance is frequently negative. An important feature is that positive spikes in pure distance, representing the movement of occupation numbers inside the polytope, coincide with the times when sites 1 and 2 are maximally entangled.

can be analyzed for openness with the generalized Pauli conditions. In Fig. 2.11, we see the trajectory with femtosecond resolution for the duration of 10 ps for (a) closed and (b) open systems. Each axis represents the population in the excited states of one of the three chromophores (sites). Even though there are 6 occupation numbers, only three of them are unique since on each chromophore the occupation numbers of the orbital pairs are constrained by the exciton Hamiltonian to sum to one. The trajectory in time starts with the excitation at site 1, denoted in the figure by the big green sphere at the coordinate (1,0,0). Points along the trajectory are color coded in green and red to denote points that lie *inside* and *outside* of the polytope of pure occupation numbers, respectively. The closed system in (a) remains pure (closed) throughout its trajectory (note that all points on the trajectory are green); the exciton in (a) oscillates between sites 1 and 2, never reaching the reaction center. When

environmental noise is added through dissipation, dephasing, and sink terms, we observe in (b) that the quantum system moves immediately from a closed 1-RDM (green) to an open 1-RDM (red).

The trajectory of occupation numbers provides a visual demonstration of how environmental noise facilitates the transport of the exciton to site 3 from which it can enter the sink. Environmental noise, it has been observed, can enhance exciton transport in a quantum system [21, 22, 36]. Typically, the enhancement is characterized by the dynamics of the quantum system. The pure and ensemble sets of the 1-RDM provide a kinematic, rather than a dynamic, interpretation of the enhancement. From the 1-RDM perspective we observe that the role of the noise is to increase the size of the set of 1-RDMs that is accessible to the quantum system. The enlargement of the set of 1-RDMs arises from the violation of the generalized Pauli conditions in the presence of environmental interactions. Importantly, the change in set size is kinematic, and yet it facilitates the dynamic transfer of exciton population through the system to the sink.

2.5.2 Energy Transfer

Trajectories of the chromphore network in the space of electron occupations allows us to characterize the exciton transfer pathway with respect to the violation of GPC in the FMO. Figure 2.12 shows, for the 7-chromophore network, excited orbital occupations of sites $1, 2$ and 3 for 10 ps. Points are colored green (orange) as and when the spectrum is inside (outside) the set of allowed 1-RDMs for pure quantum states. The ground state is depicted by the Slater point $(0, 0, 0)$ and the points $(1, 0, 0), (0, 1, 0)$ and $(0, 0, 1)$ correspond to Slater determinants with the excitation on sites $1, 2$ and 3, respectively. The system is left in an ensemble of stationary states at infinite time in the presence of purely dephasing noise ($\beta = \gamma = 0$), the system staying within the pure set at all times as indicated by points in green (see figure 2.12a). Dephasing noise dampens coherences between eigenstates of the chromophore network but there is no net transfer of energy to the reaction center.

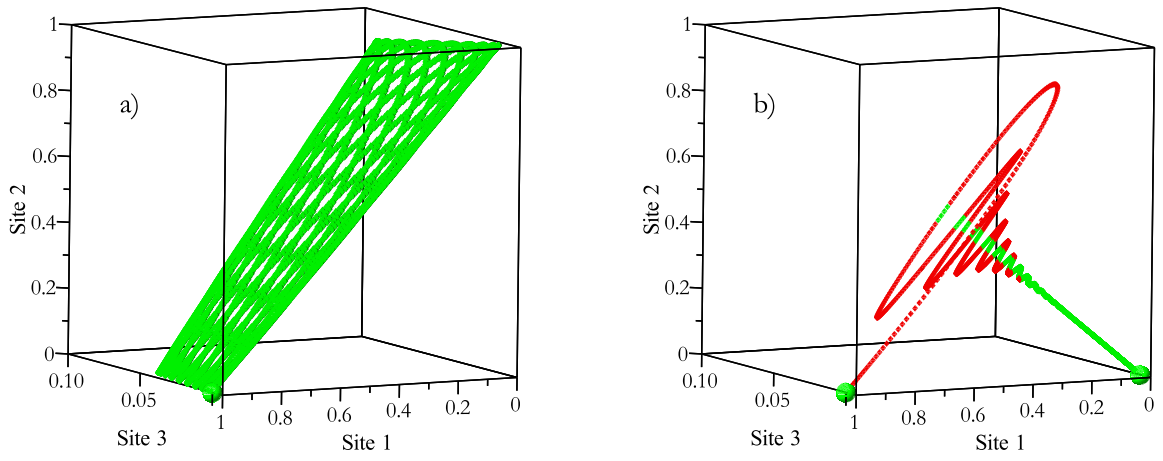

Figure 2.11: The system's trajectory in the exciton population space is shown for (a) closed and (b) open systems. Points along the trajectory are color coded in green and red to denote points that lie *inside* and *outside* of polytope of pure (closed) occupation numbers, respectively. While the closed system in (a) remains pure (close) throughout its trajectory, the open system explores a larger space of occupation numbers than the closed system as it relaxes to its ground state.

The final state of the system at 10 ps, shown by the green sphere at $(\frac{1}{7}, \frac{1}{7}, \frac{1}{7})$, is purely classical with no coherence between chromophores and the excitation is distributed evenly between the seven sites. With quantum noise (Fig. 2.12b), the FMO system begins to interact with the surrounding protein matrix and the generalized Pauli constraints relax to the Pauli constraints. As indicated by the points in orange, the spectrum of 1-RDM occupations exits outside the pure set on exposure to the environment, although it reenters the set intermittently and finishes inside the set at large times as the system relaxes to its original ground state. Transfer of energy occurs as the set of pure states relaxes to the set of ensemble states, thereby accommodating a larger set of feasible occupations. Site populations of chromophores $1, 2$ and 3 are from the full 7-chromophore FMO monomer whose spectral characterization with respect to violation (satisfaction) or of generalized Pauli constraints was performed.

The nature and the extent of deviation of the spectrum from the facets of the pure

Figure 2.12: Femtosecond trajectories of the FMO for purely dephasing noise (a) and with quantum noise where there is energy transfer to the reaction center. The spectrum is colored green (orange) when its inside (outside) the set of allowed N-electron pure states.

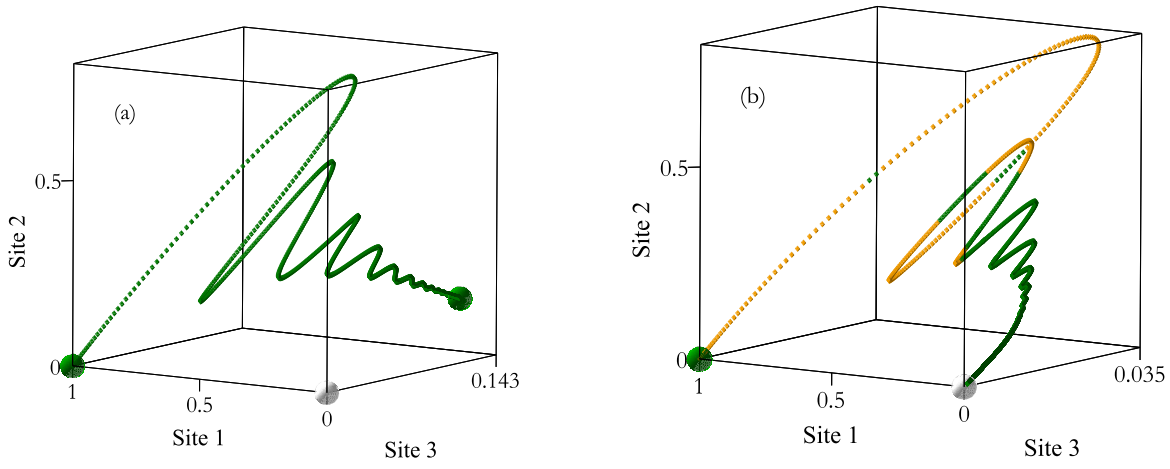

Table 2.11: Table quantifies geometry relaxation of pure quantum states during energy transfer in the FMO. With quantum noise, the pure distance (d_P) goes from 0 to negative at $50, 100$ and 325 fs. The relative dilation of pure set boundaries compared to that for mixed states, shown by $Q(t)$, turns sharply negative in the interval between 0 to 325 fs when energy transfer takes place. For purely dephasing noise, where there is no energy transfer, the pure distance stays positive and $(0 \leq Q(t) \leq 1)$ at all times.

	Dephasing Noise			Quantum Noise		
Time (fs)	$d_P(t)$	$d_E(t)$	$Q(t)$	$d_P(t)$	$d_E(t)$	$Q(t)$
0	0.0000	0.0000	1.0000	0.0000	0.0000	1.0000
50	0.0000	0.0025	0.0000	-0.0010	0.0025	-0.5140
100	0.0000	0.0019	0.0000	-0.0096	0.0018	-5.0797
325	0.0056	0.0387	0.1835	-0.0226	0.0235	-0.9621
1000	0.1101	0.1101	1.0000	0.0207	0.0207	1.0000
10000	0.1429	0.1429	1.0000	0.0009	0.0009	1.0000

set gives a quantitative estimate of the degree of interaction of a quantum system with its environment. Using a Euclidean distance metric, we measure the distance of the spectrum of occupations from the facets of the convex polytope defining the pure set [12]. This distance is positive or negative when the spectrum is inside or outside the convex polytope of occupations. For comparison we also compute distance to the ensemble boundaries given by the polytope ${}^1E_{(7,14)}$ defined by the Pauli principle on an ordered spectrum of occupations [4,

12]. Energy transfer occurs when the geometry of occupation numbers is relaxed from the pure N-representable set defined by ${}^1P_{(7,14)}$ to ${}^1E_{(7,14)}$. The extent of this relaxation is given by the ratio of pure (d_P) and ensemble (d_E) distances, Q [37]

$$Q(t) = \begin{cases} \frac{d_P(t)}{d_E(t)}, & \text{if } d_E(t) > 0 \\ 0, & \text{if } d_E(t) = 0. \end{cases} \tag{2.9}$$

which gives information, over and above the Pauli exclusion principle, about entanglement, correlation and noise in the N-electron (fermion system) [4, 12, 13, 37]. The metric Q compares the relative distance of the spectrum to the boundaries of pure and ensemble sets as a function of time and is defined to be zero for a slater determinant which is pinned to both pure and ensemble boundaries. The dimensionless quantity Q reflects the extent of violation of generalized Pauli conditions relative to the Pauli criterion and highlights the effect of the dilation of the set of occupation numbers from pure to ensemble in energy transfer. While we use the Euclidean metric to define distance to the pure set boundary, other metrics such as the trace distance or the Bures metric (related to quantum fidelity) could also be employed [38]. To remove ambiguity about saturation of GPCs calculations on the FMO were performed to a the precision of 15 decimal places.

Table 2.11 quantifies the extent of geometry relaxation of pure set 1-RDMs during energy transfer in the 7-chromophore FMO. Energy transfer occurs primarily between 0 and 1 ps after which there is little or no coherence between the chromophores. The pure distance turns negative (it is zero initially) at $50, 100$ and 325 fs and turns back positive (0.0207 at 1 ps) as the system begins to regain purity. The relative dilation of pure set boundaries relative to that for an ensemble (mixed) state is given by $Q(t)$. Q goes from goes from 1 for the original excited configuration to below zero (-0.51) at 50 fs, turning sharply negative at 100 fs (-5.0797) then back up to -0.9621 at 325 fs. Pure distance (d_P) of the system in presence of quantum noise regains positivity at longer times, reaching 0.0009 at 10 ps

(with $Q = 1$) as the system begins to relax back down its the ground (pure) state after having transferred energy to the reaction center. With purely dephasing noise, where there is no energy transfer, the pure distance stays positive at all times and $0 \leq Q(t) \leq 1$. The system is left in an ensemble of equiprobable stationary states that are equidistant to pure and ensemble boundaries at infinite time ($d_P(\infty) = d_E(\infty) = \frac{1}{7}$). In this way the geometry relaxation of 1-RDMs representing pure many-electron states in the presence of quantum noise is shown to be quantified in terms of the metric Q that turns markedly negative during energy transfer in the FMO.

2.6 References

[1] M. Altunbulak, Ph.D. thesis, bilkent university (2008).

[2] D. A. Mazziotti, Physical Review A **94**, 032516 (2016).

[3] M. B. Monagan, K. O. Geddes, K. M. Heal, G. Labahn, S. M. Vorkoetter, J. McCarron, and P. DeMarco, *Maple 2016 Programming Guide* (Maplesoft, Waterloo ON, Canada, 2016).

[4] R. Chakraborty and D. A. Mazziotti, Phys. Rev. A **89**, 042505 (2014), URL `http://link.aps.org/doi/10.1103/PhysRevA.89.042505`.

[5] M. S. Gordon and W. S. Michael (2005).

[6] M. W. Schmidt, K. K. Baldridge, J. A. Boatz, S. T. Elbert, M. S. Gordon, J. H. Jensen, S. Koseki, N. Matsunaga, K. A. Nguyen, S. Su, et al., Journal of Computational Chemistry **14**, 1347 (1993), ISSN 1096-987X, URL `http://dx.doi.org/10.1002/jcc.540141112`.

[7] C. Garrod and J. K. Percus, J. Math. Phys. **5**, 1756 (1964), URL `http://scitation.aip.org/content/aip/journal/jmp/5/12/10.1063/1.1704098`.

[8] A. J. Coleman and V. I. Yukalov, *Reduced Density Matrices: Coulson's Challenge* (Springer-Verlag, New York, 2000).

[9] D. A. Mazziotti, J. Chem. Phys **137**, 074117 (2012), URL http://scitation.aip.org/content/aip/journal/jcp/137/7/10.1063/1.4746244.

[10] W. J. Hehre, R. F. Stewart, and J. A. Pople, J. Chem. Phys **51**, 2657 (1969), URL http://scitation.aip.org/content/aip/journal/jcp/51/6/10.1063/1.1672392.

[11] R. D. Johnson, Tech. Rep., NIST (2013), URL http://cccbdb.nist.gov/.

[12] R. Chakraborty and D. A. Mazziotti, Phys. Rev. A **91**, 010101 (2015), URL http://link.aps.org/doi/10.1103/PhysRevA.91.010101.

[13] R. Chakraborty and D. A. Mazziotti, International Journal of Quantum Chemistry **116**, 784 (2016), ISSN 1097-461X, URL http://dx.doi.org/10.1002/qua.25120.

[14] R. Chakraborty and D. A. Mazziotti, The Journal of Chemical Physics **146**, 184101 (2017), http://dx.doi.org/10.1063/1.4982927, URL http://dx.doi.org/10.1063/1.4982927.

[15] R. Chakraborty and D. A. Mazziotti, Manuscript (2017).

[16] C. L. Benavides-Riveros, J. M. Gracia-Bondía, and M. Springborg, Phys. Rev. A **88**, 022508 (2013), URL http://link.aps.org/doi/10.1103/PhysRevA.88.022508.

[17] H. Kragh, Centaurus **53**, 257 (2011), ISSN 1600-0498, URL http://dx.doi.org/10.1111/j.1600-0498.2011.00237.x.

[18] C. Jungen, M. Jungen, and S. T. Pratt, Phil. Trans. R. Soc. A **370**, 5074 (2012), URL http://rsta.royalsocietypublishing.org/content/370/1978/5074.abstract.

[19] J. T. Skolnik and D. A. Mazziotti, Phys. Rev. A **88**, 032517 (2013), URL http://link.aps.org/doi/10.1103/PhysRevA.88.032517.

[20] D. W. Smith, Phys. Rev. **147**, 896 (1966), URL http://link.aps.org/doi/10.1103/PhysRev.147.896.

[21] M. Mohseni, P. Rebentrost, S. Lloyd, and A. Aspuru-Guzik, J. Chem. Phys **129**, 174106 (2008), URL http://scitation.aip.org/content/aip/journal/jcp/129/17/10.1063/1.3002335.

[22] M. B. Plenio and S. F. Huelga, New J Phys. **10**, 113019 (2008), URL http://stacks.iop.org/1367-2630/10/i=11/a=113019.

[23] M. Sarovar, A. Ishizaki, G. R. Fleming, and K. B. Whaley, Nature Physics **6**, 462 (2010), URL http://dx.doi.org/10.1038/nphys1652.

[24] N. Skochdopole and D. A. Mazziotti, J. Phys. Chem. Lett. **2**, 2989 (2011), URL http://pubs.acs.org/doi/abs/10.1021/jz201154t.

[25] J. J. Foley and D. A. Mazziotti, Phys. Rev. A **86**, 012512 (2012), URL http://link.aps.org/doi/10.1103/PhysRevA.86.012512.

[26] A. Higuchi, A. Sudbery, and J. Szulc, Phys. Rev. Lett. **90**, 107902 (2003), URL http://link.aps.org/doi/10.1103/PhysRevLett.90.107902.

[27] A. Szabo and N. S. Ostlund, *Modern Quantum Chemistry: Introduction to Advanced Electronic Structure Theory* (Courier Corporation, 2012).

[28] A. V. Sinitskiy, L. Greenman, and D. A. Mazziotti, The Journal of Chemical Physics **133**, 014104 (2010), http://dx.doi.org/10.1063/1.3459059, URL http://dx.doi.org/10.1063/1.3459059.

[29] A. A. Klyachko, J. Phys. Conf. Ser. **36**, 72 (2006), URL http://stacks.iop.org/1742-6596/36/i=1/a=014.

[30] M. Altunbulak and A. Klyachko, Comm. Math. Phys. **282**, 287 (2008), ISSN 0010-3616, URL http://dx.doi.org/10.1007/s00220-008-0552-z.

[31] G. Panitchayangkoon, D. Hayes, K. A. Fransted, J. R. Caram, E. Harel, J. Wen, R. E. Blankenship, and G. S. Engel, Proceedings of the National Academy of Sciences **107**, 12766 (2010), http://www.pnas.org/content/107/29/12766.full.pdf, URL http://www.pnas.org/content/107/29/12766.abstract.

[32] J. Adolphs and T. Renger, Biophysical Journal **91**, 2778 (2006), ISSN 0006-3495, URL http://www.sciencedirect.com/science/article/pii/S0006349506719932.

[33] S. Kais, in *Reduced-Density-Matrix Mechanics: With Application to Many-Electron Atoms and Molecules*, edited by D. Mazziotti (Wiley, New York, 2007), vol. 134 of *Adv. Chem. Phys.*, ISBN 9780471790563.

[34] R. Horodecki, P. Horodecki, M. Horodecki, and K. Horodecki, Rev. Mod. Phys. **81**, 865 (2009), URL http://link.aps.org/doi/10.1103/RevModPhys.81.865.

[35] C. C. Forgy and D. A. Mazziotti, J. Chem. Phys. **141**, 224111 (2014), URL http://scitation.aip.org/content/aip/journal/jcp/141/22/10.1063/1.4902883.

[36] K. M. Gaab and C. J. Bardeen, J. Chem. Phys **121**, 7813 (2004), URL http://scitation.aip.org/content/aip/journal/jcp/121/16/10.1063/1.1786922.

[37] F. Tennie, V. Vedral, and C. Schilling, arXiv preprint arXiv:1509.00358 (2015).

[38] H. P. Breuer and F. Petruccione, *The Theory of Open Quantum Systems* (Oxford University Press, New York, 2002).

CHAPTER 3

CONCLUSIONS

Generalized Pauli conditions arise due to the global antisymmetry of the N-fermion wavefunction and antisymmetry is the active constraint vis-à-vis energy minimization for quantum states that saturate them. At the beginning of our inquiry into their relevance for physical systems, we defined distance metrics that quantified their saturation as part of a concerted effort between 2013-2016 that has yielded consensus for the phenomenon of *quasi-pinning*, their quasi-saturation for harmonic and spin systems, and in atoms and molecules [1–3]. For open quantum systems, we defined similar saturation metrics with the additional consideration of the spectrum approaching the boundary set both from inside, as would be the case for pure states, and from outside like any measurable quantum system with noise artifacts [2]. The ratio of constraint saturation with respect to pure and ensemble N-representability conditions gave us Q, a quality factor we found to be useful in describing energy transfer in terms of dilation of the set of 1-RDMs [2, 3]. Understanding the degree to which a quantum system interacts with its environment is critical because this interaction can significantly influence its energies and properties. The openness of a quantum system can be computed through its N-electron density matrix. Determination of the N-electron density matrix by either theory or experiment, however, is challenging and difficult because the matrix scales exponentially with the system size. Using pure-state N-representability conditions (GPCs), we have shown that the openness of a quantum system is encoded directly in the 1-RDM. Unlike the N-electron density matrix the 1-RDM scales as a polynomial in the number of electrons in the quantum system. While for an open system the occupation numbers of the 1-RDM are bounded by zero and one by the well-known Pauli exclusion principle for a closed system the occupation numbers of the 1-RDM are bounded by a more stringent set of inequalities known as generalized Pauli conditions. Importantly, these generalized conditions significantly restrict the physically realistic occupation numbers for closed quantum systems beyond the usual Pauli conditions. By studying their violation for an open quantum system,

we are able to ascertain the openness of a quantum system from the 1-RDM alone.

The role of environmental interactions or quantum noise is to relax the generalized Pauli conditions, allowing the quantum system to explore a much larger set of trajectories in the natural-orbital occupation numbers. Traditionally, noise is viewed in terms of its effect on the dynamics of the system. The present work, however, shows that there is also a fundamental kinematic interpretation in terms of the geometry of the 1-RDM sets. As seen in the application to photosynthetic light harvesting, the noise expands the set of allowable 1-RDMs from its pure N-representable set to its ensemble N-representable set [1], which significantly expands the set of trajectories in orbital occupations by which the exciton can move through the chromophore network and thereby allows the exciton to travel efficiently to the reaction center for its conversion to chemical energy. The sufficient condition encoded in the 1-RDM for an open quantum system provides physical insight through its orbital occupations into the ramifications of environment interactions and openness in quantum mechanics. Experimentally, it may be possible to apply generalized Pauli conditions to probe the system-bath interactions in a variety of physical and chemical systems. The present work represents a step towards a broader use of the 1-RDM and its occupation numbers in the study of the interaction of open quantum systems with their environments.

With knowledge of GPCs, we were able to capture many-electron correlation energies from extremal single-particle occupation spectra. Pinning of the wavefunction to the boundary set $\partial\mathcal{P}^1$ of one-electron reduced density matrices provides a sufficient condition for the extremality of the 2-RDM which is a key variable is the computation of ground state energies of many-electron systems [4, 5]. This analytic a priori is validated by our numerical a posteriori presented here in that with the optimization program (1.55) that scans the pure set (polytope) boundary for the best pinned approximation to the wavefunction, we are able to: (i) recover correlation beyond the Hartree-Fock limit in the boron isoelectronic sequence, (ii) recover $> 92\%$ of the correlation energy in N_2^+ in its equilibrium geometry, (iii) qualitatively describe static correlation in linear hydrogen chains that become maximally entangled in the

dissociative limit, and, (*iv*) capture correlation in strongly entangled π systems in planar, cyclic hydrocarbons. Reconstruction of many-body states which are able to describe correlation from muti-reference effects from knowledge of single-particle marginals is significant in that it paves the way for energetic simulations of quantum states from knowledge of its 1-RDM [6, 7]. The initial success of pure state N-representability constraints in describing correlation in electronic quantum domains has inspired efforts to and formulate an efficient algorithm to enumerate GPCs for bigger systems [8, 9], an open problem at the interface of algebraic geometry and many-body physics, that will have major repercussions in quantum information theory.

We have inspected carefully the extent of GPC saturation for single-particle spectra in the electronic structure of atomic and molecular ground and excited states [1, 10, 11], and shown their violation to be sufficient to ensure openness of the many-electron quantum system [2, 3]. Using GPC facets that expose the set of pure N-representable 1-RDMs, we have shown that extremal 1-RDMs give a sufficient criterion for extremality of the 2-RDM, a key variable in quantum chemistry [5], and are able to define an energy functional that describes many particle correlation from single-particle spectra. In addition to providing a useful measure and classification of electron correlation and entanglement, the generalized Pauli conditions also offer insights into the improvement of electronic structure methods based on wave functions as well as 1- and 2-RDMs. The theorem of Hohenberg-Kohn [12] at the heart of density functional theory [13] intimates that the 1-RDM contains key elements of an atom or molecule's electronic structure including possible signatures for strong electron correlation. The generalized Pauli conditions further demonstrate that key features of electron correlation and entanglement are encoded within the 1-RDM. The definition of the set of pure N-representable 1-RDMs by the generalized Pauli conditions may provide new insights into the development of practical 1-RDM-based electronic structure methods. The generalized Pauli conditions are useful in the measurement and classification of electron correlation and entanglement, and more generally, these conditions provide fundamental insight into the

structure of many-electron quantum systems, which has been useful for both the classification and the computation of strong electron correlation.

3.1 References

[1] R. Chakraborty and D. A. Mazziotti, Phys. Rev. A **89**, 042505 (2014), URL http://link.aps.org/doi/10.1103/PhysRevA.89.042505.

[2] R. Chakraborty and D. A. Mazziotti, Phys. Rev. A **91**, 010101 (2015), URL http://link.aps.org/doi/10.1103/PhysRevA.91.010101.

[3] R. Chakraborty and D. A. Mazziotti, The Journal of Chemical Physics **146**, 184101 (2017), http://dx.doi.org/10.1063/1.4982927, URL http://dx.doi.org/10.1063/1.4982927.

[4] D. A. Mazziotti, Phys. Rev. Lett. **108**, 263002 (2012), URL http://link.aps.org/doi/10.1103/PhysRevLett.108.263002.

[5] D. A. Mazziotti, Chemical Reviews **112**, 244 (2012), pMID: 21863900, http://dx.doi.org/10.1021/cr2000493, URL http://dx.doi.org/10.1021/cr2000493.

[6] R. Chakraborty and D. A. Mazziotti, Manuscript (2017).

[7] C. Schilling, C. L. Benavides-Riveros, and P. Vrana, arXiv preprint arXiv:1703.01612 (2017).

[8] M. Altunbulak, Ph.D. thesis, bilkent university (2008).

[9] C. Schilling, Ph.D. thesis, Johannes Gutenberg-Universität Mainz (2014).

[10] R. Chakraborty and D. A. Mazziotti, International Journal of Quantum Chemistry **115**, 1305 (2015), ISSN 1097-461X, URL http://dx.doi.org/10.1002/qua.24934.

[11] R. Chakraborty and D. A. Mazziotti, International Journal of Quantum Chemistry **116**, 784 (2016), ISSN 1097-461X, URL http://dx.doi.org/10.1002/qua.25120.

[12] P. Hohenberg and W. Kohn, Physical review **136**, B864 (1964).

[13] R. G. Parr and Y. Weitao, *Density-Functional Theory of Atoms and Molecules* (Oxford University Press, 1994), ISBN 978-0-19-509276-9.